

NPS ARCHIVE  
1966  
SEARLE, H.

MEASUREMENT OF RADIANT HEAT TRANSFER  
TO THE FUEL GRAIN SURFACE IN A HYBRID  
ROCKET USING THIN FILM RESISTANCE  
THERMOMETERS

HENRY LEE SEARLE

**DUDLEY KNOX LIBRARY  
NAVAL POSTGRADUATE SCHOOL  
MONTEREY, CA 93943-5101**

LIBRARY  
NAVAL POSTGRADUATE SCHOOL  
MONTEREY, CALIF. 93940

This document has been approved for public  
release and sale; its distribution is unlimited.







MEASUREMENT OF RADIANT HEAT TRANSFER TO THE FUEL  
GRAIN SURFACE IN A HYBRID ROCKET USING THIN FILM  
RESISTANCE THERMOMETERS

by

Henry L. <sup>ee</sup>Searle  
Captain, United States Marine Corps  
B.S., University of Washington, 1956

Submitted in partial fulfillment  
for the degree of

AERONAUTICAL ENGINEER

from the

UNITED STATES NAVAL POSTGRADUATE SCHOOL  
May 1966

NPS ARCHIVE

1766

SEARLE, H.

11-11

5/1/57

5.5



TABLE OF CONTENTS

Section	Page
1. Introduction	11
2. Equipment and Instrumentation	19
3. Experimental Procedures	28
4. Results and Discussion	36
5. Conclusions	47
6. Suggestions for Further Investigations	48
7. Bibliography	50
Appendix I	81

1012-13-2101

## LIST OF ILLUSTRATIONS

Figure	Page
1. Boundary Layer Combustion Model	54
2. Burner Assemblies	55
3. Overall View of Hybrid Rocket Test Table	56
4. Cross Section of Slab Burner	57
5. Supply System Schematic	58
6. Control System Schematic	59
7. Heat Sensor Components	60
8. Complete Heat Sensor Probes	61
9. Flux Gage Bridge Circuit	62
10. Slab Grain Cross Section	63
11. Tubular Grain Cross Section	64
12. Pressure and Burning Rate Recording Circuits	65
13. Flux Gage Resistance - Temperature Characteristics	66
14. Galvanometer Sensitivity	67
15. Radiant Heat Source	68
16. Gage Temperature History from Heat Source Input	69
17. Typical Oscillograph Record	70
18. Normalized Regression Rates, Tubular Fuel Grain	71
19. Mounted Slab Grain	72
20. Oscillograph Record	73
21. Incompletely Burned-Through Slabs	74
22. Combustion Product Deposits on Gage Faces	75
23. Radiant Heat Flux/Oxidizer Flow Rate	76

# LIST OF ILLUSTRATIONS (cont.)

Figure		Page
24.	Radiant Heat Flux/Chamber Pressure	76
25.	Example of Unsteady Heat Flux	77
26.	Damaged Fairings and Aft Closure	78
27.	Destroyed Gage	79
28.	Heat Flux Parameter $\alpha_{nz}$	80

# TABLE OF SYMBOLS

Symbol	Definition
$B$	mass transfer parameter
$b$	fuel slab grain width
$c$	specific heat capacity of flux gage substrate material
$c^*$	characteristic velocity
$D_c$	sonic choke throat diameter
$D_f$	final port diameter of fuel grain
$D_o$	initial port diameter of fuel grain
$D_t$	nozzle throat diameter
$d_1, d_2$	depth to light sensor probe
$d_f$	depth to flux gage face
$G$	total mass flow rate per unit area (mass flux)
$G_o$	oxidizer mass flow rate per unit area
$G_o^o$	same as $G_o$ but based on initial port diameter
$G_f$	fuel mass flow rate per unit area
$h_{veff}$	effective heat of gasification of the fuel
$k$	thermal conductivity
$L$	fuel grain length
$m$	total mass flow rate
$m_o$	oxidizer mass flow rate
$m_f$	fuel mass flow rate
$n$	particle density in gas stream
$P_c$	combustion chamber pressure in $\text{lb/in}^2$

# TABLE OF SYMBOLS (cont.)

Symbol	Definition
$P_a$	atmospheric pressure
$P$	combustion chamber pressure in atmospheres ( $P_c/P_a$ )
$P_o$	oxidizer supply reservoir pressure
$Q_c$	convective heat transfer rate per unit area (heat flux)
$Q_g$	heat flux rate calculated from flux gage temperature history
$Q_r$	radiative heat flux rate at the fuel surface
$R$	Resistance
$R_{ex}$	Reynold's number based on length
$r$	burning rate
$T_a$	atmospheric ambient temperature
$T_r$	flame temperature
$T(t)$	flux gage element temperature increment
$t_b$	burning time
$t_s$	slab fuel grain thickness
$v$	gas velocity in the combustion chamber (average)
$W_o$	initial fuel grain weight
$W_f$	final fuel grain weight
$z$	optical path length
$\alpha$	empirical constant
$w$	emissivity of fuel surface
$\beta$	pressure exponent
$\mu$	gas viscosity

# TABLE OF SYMBOLS (cont.)

Symbol	Definition
$\rho_v$	density of fuel grain
$\rho$	density of flux gage substrate material
$\sigma$	Boltzman constant
$\lambda$	integrating variable





## 1. Introduction

The combination of liquid oxidizer and solid fuel, the hybrid rocket, has been studied for some time and has reached at least a modest level of development at the present. The interest in this type of rocket motor stems from its relatively simple thrust modulation and restart capabilities. Performance superior to that of a solid (composite propellant) rocket has been theoretically predicted, but has not been generally realized. <sup>\*</sup> Oxidizer injector design, fuel grain shape, mixing chambers, and a variety of other engineering development problems have been studied and full scale motors are being flown in operational vehicles.

Despite this appearance of progress, much remains to be learned regarding the fundamental processes involved in the hybrid rocket. Only a limited amount of research in the field was conducted prior to 1960, but in the early 1960's the Navy awarded research contracts to five major companies. Feasibility studies,  $\overline{\angle 3,5}$ , fuel-oxidizer optimization studies,  $\overline{\angle 4,5}$ , small scale testing,  $\overline{\angle 6}$ , basic combustion problem studies,  $\overline{\angle 7,9,12}$ , and analytical investigations,  $\overline{\angle 8,10}$ , were reported as a result of these contracts. Combined analytical and experimental work has been given extensive effort for the purpose of creating a theoretical model of the hybrid combustion problem that is valid for a wide range of fuel-oxidizer combinations and operating conditions  $\overline{\angle 8,10,16,17}$ . References 18 and 19 contain surveys of the literature of recent years.

\*Numbers in brackets indicate references listed in the Bibliography.

Obviously, an accurate analytical description of the hybrid combustion process would be of inestimable value. Such a description has as its end the prediction of the burning rate, given the properties of the fuel and oxidizer and the operating conditions. To date no completely satisfactory theory has been developed, although several have been proposed. The most significant of the theoretical analyses have been presented by Marxman, et al, of United Technology Center, Sunnyvale, California; and by Smoot of Lockheed Propulsion Company, Redlands, California. These analyses involve what has become the accepted model as illustrated in Fig. 1. Turbulent boundary layer flow, or fully developed turbulent pipe flow, of the oxidizer over the fuel is assumed with combustion taking place in a thin flame zone within this boundary layer. Heat transferred to the fuel surface from the flame gasifies the fuel. Diffusion of the fuel and oxidizer is commonly considered to be the rate limiting consideration for the combustion process. For some fuel-oxidizer combinations and operating conditions there is evidence of other rate controlling mechanisms such as heat transfer rates, gas phase chemical kinetics, and surface reactions. The apparent presence of these other mechanisms prevents, at the present time, the wholehearted adaptation of any of the available analytical descriptions of the process. Much work remains to be done to further verify or to improve these analyses.

In the analysis given by Marxman the principal parameters involved in the regression rate (for a given fuel-oxidizer combination) are pressure, flame temperature, and fuel grain geometry.  $\sqrt{10}$  These parameters are

inter-related and do not appear directly in the burning rate equation. The burning rate is given by

$$r = \frac{\dot{Q}_c}{\rho_s h_{veff}} \left[ \frac{\dot{Q}_r}{\dot{Q}_c} + e^{-\frac{\dot{Q}_r}{\dot{Q}_c}} \right] \quad (1)$$

where  $\rho_s$  is the solid fuel density, and  $h_{veff}$  is the effective heat of gasification of the fuel. The other quantities are defined in the Table of Symbols, page 7. The radiative and convective components of heat transfer are given by

$$\dot{Q}_c = h_{veff} \left[ 0.036 B^{0.23} P^{0.23/\beta} G R_{ex}^{-0.2} \right] \quad (2)$$

and

$$\dot{Q}_r = \sigma \epsilon_w T_r^4 \left[ 1 - e^{-\alpha n z} \right] \quad (3)$$

respectively. In Eq. (3), it is necessary to estimate, or determine experimentally, values for  $\alpha$ ,  $n$ , and  $z$  as well as  $\epsilon_w$  and  $T_r$ .

For certain fuels, notably those with no solid phase combustion products, the radiation heat transfer term can be neglected and Eq. (1) becomes

$$r = \dot{Q}_c / \rho_s h_{veff} \quad (4)$$

However, for fuels with metal particle loading, and for some polymeric binders, the combustion products will include solid particles which will produce significant radiation at the flame temperatures involved. This would seem to indicate that the radiative system will be typical of practical hybrid fuels. [15,19]

For a hybrid system the convective and radiative heat transfer mechanisms are physically coupled. An increase in radiation increases the heat transfer to the pyrolyzing wall and tends to increase the mass flux away from the fuel surface. This increased mass transfer acts to block the convection of thermal energy to the fuel surface. The formulation of Eq. (1) has attempted to include this coupling.

To date no adequate method has been devised to experimentally determine the values of  $\dot{Q}_c$  and  $\dot{Q}_r$ . Values for these two heat transfer components are established from a combination of assumptions and empirical data in an iterative calculation of burning rate using Eq. (1). The total heat transfer ( $\dot{Q}_c + \dot{Q}_r$ ) can be verified adequately from experimental burning rate data using established values for the heat of gasification of the fuel, but the value of the individual components is of particular interest as a verification of the validity of the form of Eq. (1).

Flame temperature measurements have been reported wherein thermocouples of tungsten-tungsten-10 percent rhenium were inserted into the flame zone of a plexiglas-oxygen system. [7] The oxidizer was oxygen diluted with nitrogen and the results, plotted in the form  $T_f$  versus oxygen concentration, were extrapolated to 100% oxygen. Results indicate that



$T_r$  for this system should be of the order of  $2600^{\circ}\text{K}$ . Variation in this temperature is expected with position in the grain due to change in stoichiometry. The emissivity of the wall can be reasonably estimated but the values of  $\alpha$  and  $n$  are not so well bounded. Additional problems arise from the unknown optical properties of the boundary layer between the flame and the wall. Thus it appeared desirable to attempt to determine directly the amount of radiant energy reaching the wall.

### Radiation Heat Transfer Measurement

Radiation heat transfer methods generally are cumbersome and plagued with difficulties regarding optical properties of the measuring device, the radiator, and the intervening material.

The hybrid rocket heat transfer problem possesses additional difficulties of its own. For example, results are reported for total radiation measurements using clear inserts in plexiglas and polystyrene fuel grains.

[7,9,12] A thermopile pyrometer was used as the measuring device in these atmospheric pressure experiments. These experiments were hampered by fogging of the viewing window by soot deposition during the long viewing time required by the instrumentation.

The intensity of radiation depends upon the concentration of radiators in a flame. As a consequence it might be expected that a strong pressure dependence will exist in the radiation heat transfer term. Hence the problem of working through the boundaries of a pressurized combustion chamber is present, if this pressure dependence is to be verified.

If the radiation sensor is to assume the viewpoint of a portion of the fuel surface, it must be capable of doing its job in the environment to which the wall is exposed. This means that it must withstand exposure to a reducing atmosphere at high temperatures. The distance from the wall to the flame zone can be expected to be of the order of 0.01 inches and the flame temperature probably exceeds  $2500^{\circ}\text{K}$  under most conditions. The surface temperature of the wall is the boiling point or gasification temperature of the polymeric fuel, generally of the order of  $400\text{--}800^{\circ}\text{F}$ .

The surface of the fuel is not stationary, but is regressing at some finite rate. There is, then, some difficulty associated with the location of the fuel surface at any given time.

With these problems in mind, it is appropriate to examine the various instruments used for measuring radiation energy with the intent of selecting the most suitable. Some of these instruments (such as thermopile pyrometers, and photosensitive pyrometers) are eliminated immediately, because of the geometry of the sensor, or their slow response time. The bolometer, a comparative resistance thermometer, is also essentially a steady state device and does not seem to have the fast response necessary.

The thin film resistance thermometer is a relative newcomer in the field of radiation measurements. This device was developed as a means of instrumenting the typically minute models in shock tube wind tunnels. [1] From shock tube application also came the requirement for response times of the order of 0.001 sec. Use of the thin film resistance thermometer as a radiation sensor is described in references 11, 13, 20, and 21 in

connection with shock tube studies of rocket base heating. The response rate of this sensor is quite fast compared to the regression rate of the hybrid rocket wall. For example, if the fuel surface regresses at 0.10 in./sec, it will advance only 0.0001 in. during one millisecond. Thus, the fuel surface may be considered to be stationary during the time required for the sensor to respond. The thin film resistance thermometer is small enough to be mounted inside the pressure enclosure and is adaptable to protection from the hostile environment without serious detriment to its performance. Optical property difficulties normally associated with radiation measurement apply to this device and it has some other peculiarities, but nevertheless it seemed worthwhile to attempt to apply this instrument to the investigation of hybrid rocket combustion phenomena.

In this application of the thin film resistance thermometer (which will be referred to as a flux gage for convenience) several problems are anticipated and must be overcome if success is to be realized.

First, the gage must be protected from convection and conduction heat transfer if the output is to represent radiation. This protection can be accomplished by placing a window of transmitting material between the source of thermal energy and the gage film. This window must, of course, transmit in the infrared and near infrared wave lengths. Several materials are suitable including Pyrex, fused silica, and synthetic sapphire. Of these, clear fused silica (quartz glass) was determined to be the most practical. The passband (50% points) of fused silica is 0.20 to 4.0 microns

and the transmissivity of a 1/16-inch thick fused silica window is shown to be 0.935 in Appendix I.

The probability that the protective window will be clouded by deposition of combustion products is also anticipated. This is the principal reason for requiring instrumentation with short response time. The object in this regard is to gather the data desired in the short time between exposure of the viewing window and the obscuration of the window by combustion products.

In addition, there are difficulties involved in the selection of material for construction of the "probe" which will hold the gage in position inside the rocket motor. These materials will be exposed to the same hostile environment as the gage and are required to withstand these conditions long enough to allow the gage to function. Ideally, the flux gage and associated mounting should be reuseable for more than one experiment without major repairs.

Information is obtained from the flux gage in the form of a temperature history. Conversion of this temperature history to a value of heat flux at the fuel surface requires the invocation of linear one-dimensional heat conduction theory as applied to a semi-infinite solid. A derivation of the necessary equations after Vidal appears in Appendix I.  $\overline{[1]}$  The resulting equation for heat transfer rate in terms of temperature history is

$$\dot{Q} = \frac{\sqrt{\pi \rho c k}}{2} \left[ \frac{T(t)}{\sqrt{t}} + \frac{1}{\pi \sqrt{t}} \int_0^t \frac{\sqrt{\lambda} T(\lambda) - \sqrt{t} T(\lambda)}{(t - \lambda)^{3/2}} d\lambda \right] \quad (5)$$



where  $T_{(t)}$  is the increment of temperature above that of the gage element at  $t \leq 0$ .

After calculation of the heat input to the gage element using Eq. (5) it is necessary to correct for the reflectivity of the platinum film, and for the radiation energy absorbed and reflected by the protective window. Bogdan has shown that forty percent of the radiation incident upon a bright platinum film will be absorbed by it. The window transmits 93.5% of the energy radiating to its outer surface, so that the radiant heat transfer to the protective window surface is given by

$$\dot{Q}_r = \frac{\dot{Q}_{gage}}{0.374} \quad (6)$$

The intent of this present investigation then was to determine the feasibility of obtaining quantitative information regarding radiant heat transfer to the solid fuel surface in a hybrid rocket by utilizing thin film resistance thermometers and linear, one-dimensional heat conduction theory.

## 2. Equipment and Instrumentation.

### Hybrid Rocket Test Table

The apparatus for these experimental studies was designed and constructed at the United States Naval Postgraduate School, Monterey, California. The apparatus consists of a tube burner assembly, a slab burner assembly (Fig. 2), and associated supply and instrumentation systems. For convenience these burner assemblies were mounted on a 30-inch by 72-inch steel frame table (Fig. 3). The provision of disconnecting points at the

table allows portability without the requirement for disruptive disassembly of the system. Control and instrumentation components were mounted on the test table or on roll-away instrument carts.

The tube burner assembly was employed as described by Lousma [19]. This assembly (constructed of stainless steel) consisted of an injector, aft support, nozzle retainer clamp and supporting structure. A brass flow straightening section was added to help assure fully developed pipe flow throughout the burner section. Oxygen was supplied through a one-half-inch port in the injector. The propane and oxygen used for ignition were injected through one-eighth-inch ports in the injector. Ports for chamber pressure and purging nitrogen were placed in the wall of the brass flow straightening section. O-rings provided pressure seals at the ends of the fuel grain.

The slab burner assembly required significant amounts of engineering and machining effort. The structure was designed to withstand an internal pressure of 1000 psi, and constructed of mild steel. The slab burner consisted of top and bottom pieces, aft closure assembly, and side closure plates. Sealing was accomplished by using 1/64-inch thick Armstrong #167 cork and neoprene composition gasket material. The aft closure assembly included provisions for circulating cooling water around the nozzle insert to prolong nozzle insert and gasket life, and to reduce the cool down time required after firing before disassembly. Ports were provided in the head end of the assembly for the introduction of propane, oxygen, nitrogen and air, and for the line to the chamber pressure transducer. The aft closure assembly was machined to receive the same graphite nozzle inserts as were used in the tube burner assembly.

The internal configuration of the slab burner was designed to provide flexibility in the type and size of fuel grains utilized. Basically, provision was made for two one-half inch thick slabs, two inches wide. Steel inserts were constructed to produce a straight flow passage while utilizing only one slab at a time, and/or thinner ( $1/4$ " ) slabs. By making slight modifications to these inserts a variety of grain geometries can be accommodated. The particular slab configurations used in this study will be described in the section entitled Fuel Grain Preparation.

The heat flux sensor was inserted through a  $37/64$ -inch hole drilled through the top piece of the burner. A corresponding hole in the filler plate allowed the flux gage holder to be inserted into the grain itself. The hole in the slab burner top piece was tapped with  $3/8$ -inch taper pipe threads, and a brass and neoprene ferrule tube fitting was screwed in to anchor and seal the shaft of the flux gage holder. A transverse cross section of the slab burner, illustrating these details, appears in Fig. 4.

It was considered desirable to obtain local burning rate data in the vicinity of the radiation measuring probe. By this means any disturbance in regression rate caused by this foreign "inclusion" in the grain would be detected and could be accounted for in the analysis of results. For burning rate measurements, light conducting passages were provided through the burner walls (and the inserts) to light detecting resistors mounted in a phenolic holder fastened to the burner. These light passages were made by cementing tapered polystyrene rods into drilled and taper reamed holes with an epoxy cement.

To insure adequate gasket compression for seal, the slab burner assembly was assembled with a measured bolt torque of 150 inch pounds. Using criteria recommended by the gasket manufacturer, this was expected to yield a flange pressure of  $1200 \text{ lb/in}^2$ . The bolts used were of high strength forged steel. Bolt tension, cold, at 150 inch pounds torque was calculated to be 900 lb. Additional tension due to pressure in the most highly stressed bolt at  $1000 \text{ lb/in}^2$  internal pressure was 482 lb. for a total maximum bolt load of 1382 lb. Allowable load for these bolts 3840 lb.

The slab burner was tested for static seal integrity using a dead load hydraulic pressure of 500 psia. The seal integrity was checked again after each disassembly by inserting an undrilled nozzle insert and pressurizing with nitrogen to 300 psia.

The oxidizer supply system consisted of a Victor Simplex manifold connecting three high pressure oxygen cylinders to a Victor GD10-967 Regulator. Oxygen flow was routed through a metering device (Sonic Choke) and a solenoid valve to the injector of the burner assembly in use. Nitrogen, used as a purge to insure extinguishment, was supplied through a Hoke Phoenix pressure regulator and a solenoid valve. Propane and oxygen for ignition were supplied through solenoid and throttle valves to the injector of the burner assemblies. A spark plug and coil system was used for ignition of the propane-oxygen mixture. Supply and control systems are shown schematically in Figures 5 and 6.

#### Heat Sensors

The thin film resistance thermometers chosen for this work were supplied gratis by Cornell Aeronautical Laboratory (CAL). The gage itself



consists of a thin platinum film deposited on a Pyrex or fused silica substrate. Although several methods of depositing the platinum on the glass have been investigated, the most feasible seems to be that of brushing on a metal solution and baking or firing in an oven. 17 The metal solution used for these gages was Hanovia Liquid Bright Platinum 05X. Firing temperature depends upon the substrate material, the requirement being a temperature near the softening point of the glass. Several sequences of brushing and firing may be required to obtain the desired resistance, i.e. within 25% of 100 ohms. The six gages received from CAL varied in resistance from 82.78 to 105.61 ohms at 71 degrees F. The finished element is about 0.025 in. wide by four micro-inches thick. A coating of magnesium fluoride is deposited on the face of the instrument to provide electrical insulation and physical protection. This coating is typically about four microinches thick. Lead wires are attached by soldering and the sensor is mounted into a holder, or in some cases, installed directly into the model. 17

The resistance of the gages is a function of temperature and tends also to be a function of temperature history. Resistance films produced by the firing technique show less instability than evaporated films, because of the annealing effect of the firing cycle. 117 Consequently additional "annealing" cycles are useful after the final coat of metal solution is fired. This process consists of heating the gage to a high temperature (perhaps 200°F below the softening point of the glass) for several hours, followed by a slow cooling (10 or 12 hours). Two of these thermal cycles generally suffice to stabilize the gage resistance-temperature characteristics.

The gages received from CAL were permanently mounted in brass fittings as shown in Fig. 7. For this study it was necessary to devise two types of holders to accommodate these brass fittings and adapt them to the conditions imposed, that is to facilitate application to the slab burner or to the tube burner. The holder for the tube burner application appears in Figures 7 and 8 and the holder used in the slab burner is illustrated in Fig. 8. These holders were machined from cotton-phenolic rod. The mounted sensors and the windows were cemented into the holders with an epoxy resin (APCO 210).

The windows used in this application were manufactured from Corning #7940 fused silica. The windows were ordered flat to one wavelength in the visible band, but considerable difficulty was experienced by the supplier in polishing these small ( $7/16$ " diam.,  $1/16$ " thick) windows to that quality. After some discussion with the supplier, it was decided that in the interests of time and economy a reduced optical quality would be accepted. As a result of this the windows used were of variable flatness, the extremes being flat to one wave and just pitch-polished commercial grade. It is believed that no serious detriment to the work resulted from this decision. It should be noted here that "flat to one wavelength" is a rather high degree of quality in optical material, suitable for Schlieren photography and similar applications. It was necessary to exercise care in bonding the glass into the holder so as to avoid either an excessive airspace or a layer of epoxy between the window and the gage.

The anticipation of pressures up to 30 atmospheres in the burner chambers required considerable care in devising a method of introducing

the heat sensors into the fuel grain wall. In the case of the tube burner the heat sensor holders were held in place by the specially prepared phenolic fittings and an ordinary 4-inch "C" clamp. A positive seal was assured by cementing the heat sensor holder into the recess bored in the fuel grain.

In the slab burner, the mounted flux gage was not cemented into the milled recess in the fuel grain, because the small surface area available in the slab grain was not adequate for seal. Sealing in this case was provided by a neoprene ferrule tube fitting secured about the shaft provided on the flux gage holder (Fig. 4).

#### Heat Sensor Instrumentation

The resistance thermometer is a passive sensor and requires an external source of electrical power. The essential features of the electrical circuitry used with the resistance thermometers in this investigation are shown in Fig. 9. The power supply used was a Hewlett Packard Model 721A Transistor Power Supply. The bridge circuit had the property that a change in resistance of the sensor resulted in a proportionate voltage increment appearing across the input terminals of the Honeywell Model 1508 Visicorder galvanometer. The potentiometer in series with the galvanometer provided for adjustments of the sensitivity of the recorder trace (inches displacement per millivolt input). The galvanometer used was a Honeywell Series M Subminiature Type No. M400-120. It had a flat ( $\pm 5\%$ ) frequency response up to 240 cycles/sec, nominal coil resistance of 112 ohms, and a nominal sensitivity of 0.116 in/mv. Use of the

recording oscillograph provided a continuous record of gage resistance during the firing of the burner and thus a record of gage temperature. It was necessary to use a relatively high chart speed (10 in. per sec.) to obtain a useable record of the increment at gage exposure.

Considerable effort was expended in calibrating and preparing circuitry for utilization of a Tektronix Type 545 Oscilloscope and Dumont/Polaroid Oscilloscope camera to record the flux gage output. The capability of using AC amplification with the oscilloscope would have been advantageous.  $\sqrt{2}$  A high noise level in the scope, probably due in part to the long loop formed by the gage leads and in part to the presence of other equipment (such as the timer trace in the Honeywell Visicorder) caused difficulties with triggering stability in the delay mode of the oscilloscope. These problems led to abandoning the oscilloscope in favor of the Honeywell oscillograph.

#### Auxiliary Instrumentation

Burning rates were obtained initially by means of one-eighth-inch diameter clear inserts in the fuel grain. These inserts were of clear epoxy resin injected into holes bottom-drilled to carefully determined depths. Figures 10 and 11 are cross-section views of the prepared grains and the preparation is described in detail later. As the regressing fuel grain surface uncovered the ends of the transparent probes, light was transmitted to Lafayette Model PC 41 cadmium sulfide photoconductive cells mounted in a Micarta clamp on the outer surface of the fuel grain. Response time of the light sensors was ten milliseconds.



The light sensors were actuated in pairs by a 6 volt dry cell battery in the circuit shown in Fig. 12. The Honeywell oscillograph was used to record the output from the light sensors.

Combustion chamber pressure was measured through ports in the injector end of the respective burner assemblies. This pressure line was connected both to a Wiancko 300psig Type P-2-3086 transducer and to a standard Ashcraft direct reading 0-500 psig gage. A pressure tap was also provided in the oxidizer reservoir and a Wiancko 1000psig Type P-2-1251 transducer was connected to the reservoir in addition to the Marsh Master Test gage previously installed. These pressure transducers were powered by a 28 volt Trygon DC power supply and connected as shown in Fig. 12 to the Honeywell oscillograph for output recording. The galvanometers installed in the oscillograph for use with the transducers were Series M Subminiature Type 400-120, capable of 240 cps frequency response. This frequency response was considered adequate to record pressure fluctuations due to low frequency combustion instability.

Burning time was obtained by connecting a Yellow Springs Instrument Co. Model 105 Electrical Test Interval Measuring Timer into the control circuit in such a way that the oxygen control switch activated the timer. Thus the burning times recorded represent the time interval during which oxygen was being supplied to the burner. The Model 105 timer is accurate to 0.001% of a timed event or 0.001 second, whichever is larger. It displays seconds and tenths of seconds on a mechanical counter and hundredths and thousandths of seconds are indicated by two columns of neon lighted digits.

### 3. Experimental Procedures.

#### Fuel Grain Preparation

Two fuel configurations were utilized: molded tubular grains, nominally two inches outside diameter by eight to twelve inches long, were used in the tube burner, and slabs milled to 0.25 by 1.25 by 7.00 inches were used in the slab burner tests. Fuels were clear polymethylmethacrylate (plexiglas), clear polystyrene, 40% and 20% aluminum filled plexiglas, and black (0.5% Carbon Filled) polystyrene. The clear plastic fuels were utilized for equipment check out and calibration.

Preparation of the fuel grains for the heat transfer measurement tests consisted of installation of light sensor probes for burning rate measurements, and machining of the recess for the flux gage holder.

A cross section of the prepared slab appears in Fig. 10. The grain preparation began with milling to the external shape and dimensions. This was followed by drilling the two small flat bottomed holes to receive the light sensor probes. This was done on a milling machine with the intent of having the remaining thicknesses of the slab 0.031 inch and 0.062 inch respectively. Measurement after the work was completed revealed that the undrilled thicknesses were between 0.029 and 0.032 for the deep hole and 0.057 to 0.060 for the other. These values were recorded for each grain, obviating the necessity for concern with the variation from grain to grain. The bottom-drilled holes were filled with a transparent epoxy so that as the opaque wall burned away and uncovered the probe, light would be transmitted to the photoconducting cells mounted outside the burner walls.

Finally a 9/16-in. diameter recess was milled into the slab to a depth of 0.188 in. (remaining thickness  $0.061 \pm 0.001$ ) to receive the heat sensor holder and the weight of the grain to the nearest 0.1 gram was recorded. The heat sensor recess and the light sensor probes were located at a point 4-5/8 inches from the leading edge of the grain.

The tubular grains were prepared from two-inch diameter cast polystyrene rod. After cutting to length (8 and 10-inch lengths were used) a one-half inch hole was bored lengthwise along the rod axis. The cylinder thus formed was placed on a mandrel and the outer surface was turned on a lathe to insure that the outer and inner walls of the cylinder were concentric. At a point 3-1/2 inches from on end of the grain a pair of light probes were installed much as described above. The probes were spaced  $45^\circ$  apart on the same meridian and were bottom drilled to depths of 0.625 and 0.656. The holes were filled with transparent epoxy resin. At a point 5-1/2 inches from the head end of the grain a recess 0.5625 inches in diameter was milled into the tube wall to a depth of 0.625 inches to receive the heat sensor holder. The heat sensor holder was carefully cemented into place to insure a pressure seal and the weight of the grain was obtained to the nearest 0.1 gram.

#### Instrument Calibration

Calibration of the auxiliary instrumentation, the equipment utilized to obtain pressures and burning rate information, was a routine task involving only standard methods related to the equipment. The pressure transducers were checked against a Marsh Master Test Pressure gage as a

standard and the necessary adjustments were made at the oscillograph to obtain the desired sensitivity. After initial calibration it was necessary before each test only to check the zero point of the transducers after allowing an adequate warm up period. Some non-linearity existed in the pressure recording circuit, but the system yielded data accurate to within three percent.

The sensing circuit for the photo-conductive cells required no calibration as such. It was necessary only to design the circuit to yield the desired trace on the record and to check it before each test for circuit continuity. The one quantitative aspect of the light probe trace record was the linearity of chart speed. The Honeywell oscillograph was demonstrated to be quite adequate in this regard by comparing chart time grid traces with the test interval timer.

Obtaining accurate, useful information regarding radiation heat flux from a platinum film resistance thermometer was not a "routine" task, but rather required extensive attention to details of gage and instrument calibration and test execution. Two principal items of information must be known about the gage itself; the slope of the resistance-temperature curve ( $\frac{dR}{dT}$ ) and the value of the parameter  $(\rho ck)^{1/2}$  and its variation with temperature. Here  $\rho$  is density,  $c$  is specific heat and  $k$  is thermal conductivity of the Pyrex substrate.

The value of  $(\rho ck)^{1/2}$  can be determined by exposing the gage to a known, constant heat flux and recording the transient surface temperature. By using short test times and small temperature increments the data are



interpretable from linear one dimensional heat conduction theory applied to a semi-infinite body.  $\sqrt{1}$ . The governing relation is

$$T(t) = \frac{2 \dot{Q}_r t^{1/2}}{(\pi \rho c k)^{1/2}} \quad (7)$$

where  $T(t)$  is the transient surface temperature increment,  $\dot{Q}_r$  is the heat transfer rate (constant), and  $t$  is time.  $\sqrt{1}$  The value of  $(\rho c k)^{1/2}$  is easily calculated from the measured values of  $T(t)$ ,  $\dot{Q}_r$ , and  $t$ . The experimental determination of  $(\rho c k)^{1/2}$  is described in detail by Bogdan in Ref. 13. Data applicable to the gages used here is also published in Ref. 13. There is little variation in  $(\rho c k)^{1/2}$  from sample to sample of a particular material, so that calibration of individual gages is unnecessary.

Although each gage will have a unique value of sensitivity at a given temperature, the variation of sensitivity with temperature is given by a single equation for all gages of the same material. However, for small temperature changes  $dR/dT$  may be considered constant. The value of  $dR/dT$  was verified for each of the six gages received from CAL and the resulting data are plotted in Fig. 13.

When current is passed through the resistance thermometer there is a temperature rise due to the electrical energy dissipated in the gage. This rise can be easily determined or in some cases ignored. In this case (using a 12 volt power supply), the steady state temperature was determined to be about 100 degrees F. above ambient. This temperature was determined for each gage by allowing an adequate warm up period,

rebalancing the bridge , and then replacing the gage with a decade resistance box to determine the resistance of the gage branch at bridge balance .

The term "steady state" in this case is a slight misnomer . Variations in gage temperature are influenced by a variety of factors other than the current flowing through them such as the temperature of the interior of the burner assembly and the time elapsed since the last test . Hence it was considered advisable to determine the resistance of the gage at the balanced bridge condition before each run .

Variations in the gage resistance at the beginning of the test had negligible effect on the recorder sensitivity as is shown by Fig. 14 . The galvanometer response was nearly linear for the full scale deflection over a broad range of gage resistances at bridge balance .

Two methods of obtaining a radiant heat source of sufficient magnitude and reliability were tried . Photographic flash bulbs (No. 5) were first used . These bulbs have a rise time of 20 milliseconds to peak visible output . To obtain a shorter rise time in the heat input , a 750 watt projection lamp was finally selected as a radiation source . This lamp was mounted in the device shown in Fig. 15 . A 9/16-inch hole in the side of the three-inch diameter aluminum chimney allowed the flux gage to view the lamp element from a known distance . A first approximation to the heat flux at the gage face yielded a value of  $3.5 \text{ BTU/ft}^2 \text{ sec}$  which was about one fifth that expected in the hybrid rocket . Exposure was accomplished by removing an insulated opaque panel from a position between the gage and

the window in the chimney. "Shutter" time was estimated to be less than two milliseconds.

In Fig. 16 is shown a typical trace of the gage output on exposure to the projection lamp. Application of Eq. (5) to this curve yields a value of  $2.8 \text{ BTU/ft}^2 \text{ sec}$ . This value was repeatable and applicable to all the gages used in these tests, indicating that the projection lamp was a reasonable choice as a "known" source.

The sensitivity of the oscillograph trace to bridge imbalance was made adjustable by including a 20 turn  $10 \text{ k}\Omega$  potentiometer in series with the galvanometer and its shunt resistance. After initially adjusting this sensitivity simply in terms of galvanometer voltage drop per inch deflection, it was determined that the necessary multipliers to convert the galvanometer voltage to temperature could be put into the sensitivity adjustment. Thus the oscilloscope trace would represent gage temperature directly.

### Laboratory Technique

The experiments conducted categorize conveniently into preliminary studies and fully instrumented experiments. The preliminary tests were necessary to verify the operational condition of the apparatus and to verify the effectiveness of the ignition technique for various fuels and chamber conditions. Chamber pressure, oxidizer reservoir pressure, and burning rate data were also obtained during these experiments for use as a basis for selection of nozzle throat diameters and sonic "choke" diameters. Fully instrumented experiments were those in which one of the six available

flux gages was installed. The technique described will be that for a fully instrumented experiment.

A data sheet (Table I) was prepared prior to reaching the laboratory. Upon reaching the laboratory the power supplies, the timer, and the oscillograph were turned on. The flux gage to be utilized was connected into the bridge circuit and the circuit activated to commence gage warm-up. The burner assembly in use was then checked for condition of O-rings and gaskets, and the appropriate fuel grain was installed. The burner was assembled and, in the case of the slab burner, the bolts tightened uniformly with a torque of 150 in-lbs.

Determination of the desired nozzle throat diameter was made by calculating  $c^*$  from previous data and solving the "choked flow" equation for  $D_t$ :

$$D_t = 2 \sqrt{\frac{c^* \dot{m}}{\pi g R_e}} \quad (8)$$

A plot of chamber pressure versus throat diameter with oxidizer mass flux as a parameter was easily constructed from preliminary data. This graph facilitated selection of nozzle throat diameter during subsequent experiments.

A daily check of the pressure transducer circuit was made by pressurizing the chamber pressure and oxygen transducer lines with nitrogen to the maximum capability of the chamber pressure transducer (300 psig). The March Master test gage was used as the basis of



calibration. Day to day variation in the system was found to be insignificant.

The response of the flux gage was checked by exposing it to the lamp source and then the gage was installed in the burner. (This was not possible in the tube tests since the gages had to be cemented into place at least 24 hours before the test.) The light sensors were then mounted, the appropriate sonic choke was installed, the supply valves (water, propane, nitrogen, and oxygen) were opened, and the regulators were set at the desired values. Oxygen supply pressure was verified by activating the oxygen switch while observing the galvanometer trace on the oscillograph. After resetting the timer to zero, the apparatus was ready to operate.

The test sequence was initiated by activating the master switch, cooling water switch, and the oscillograph. The ignition switch was then held on until flame was observed at the nozzle, and then the OXYGEN/NITROGEN switch was turned to OXYGEN, and the ignition switch released. At the termination of the test the OXYGEN/NITROGEN switch was pulled through the OFF position to the NITROGEN position to extinguish the flame and purge the motor. The air valve was then opened and the nitrogen turned off. Cooling water and air were allowed to flow to cool the burner.

The oscillograph record was exposed to the Latensifier light to develop the traces and the grid, and then either rewound on the take-up reel or stored in a light proof envelope.

Finally, the fuel grain was removed from the burner, weighed, measured, and inspected for visual indications of burning characteristics.

The data sheet was completed and any unusual, unplanned, or unexpected occurrences or observations related to the experiment were recorded on the data sheet.

#### 4. Results and Discussion

The results of this experimental investigation divide conveniently into miscellaneous preliminary results, and heat transfer measurements. The discussion of preliminary results concerns principally the measurement of regression rates and the problem areas attendant to obtaining this secondary data. Under the heading of heat transfer measurement the problems encountered in obtaining meaningful data, as well as the results, will be discussed. A summary of significant data appears in Table II.

##### Preliminary Information

As has been reported previously by Lousma the tube burner performs satisfactorily in all respects. [19] The addition of the flow straightening section improved the flow characteristics within the fuel grain port. Redesign of the control and supply systems eliminated the requirement for manual control of the oxidizer supply and allowed operation of the apparatus from outside the test cell, a considerable advantage from the standpoint of safety.

The slab burner assembly also performed well in its final configuration. In all, 30 static firings were performed in the slab burner and 16 in the tube burner. The data obtained from each firing were in the form of galvanometer deflection traces on a single oscillograph chart strip and a reading from the timer.

On the chart were traces for chamber pressure , oxygen reservoir pressure , and light sensor voltage drop . (The resistance thermometer temperature trace was on this same strip for those firings which were so instrumented.) A typical oscillograph record (with a condensed time scale) is shown in Fig. 17.

The light sensor data were reduced by measuring the distance between the sensor actuation points , converting this to a time base from the known chart speed and dividing the difference in light probe depths by this time , that is:  $r = \Delta d / \Delta t$ . This burning rate measurement technique has been demonstrated to be accurate and valid and was incidental to this investigation. [19] However , as has been mentioned earlier , a slight modification to the technique described by Lousma was attempted in that epoxy light probes were used in the grains instead of plexiglas rod inserts . This technique simplified the preparation of the grain considerably . The first epoxy used was Hetron 197 , a high temperature resistant epoxy that is quite transparent when cured . This material charred so badly when exposed in the rocket motor that insufficient light penetrated to activate the sensors . Subsequently , American Plastics Company epoxy APCO 210 was used . This resin appears translucent (milky amber) when cured , but did not char and proved to be satisfactory .

In the slab burner the use of the light probe method to obtain burning rates proved to be an extremely time consuming endeavor . Combustion products accumulated on the polished interfaces of the burner light passages and obscured the passages . There was also a tendency for the

polished face of the passages to be damaged by the temperatures involved, necessitating replacement between runs. Inasmuch as satisfactory burning rate data were available by other means, the use of the light sensors in the slab burner was abandoned pending modification of the equipment.

Burning rates in the slab burner were obtained by measuring the slab thickness before and after firing and dividing this change in thickness ( $\Delta t_s$ ) by burning time:  $r = \Delta t_s / t_b$ . It was necessary to obtain an average thickness for the post-fire figure, but the grains burned very evenly and remained flat even in the vicinity of the heat flux gage recess. Burning rate was also calculated from the change in weight of the grain. This rate was generally higher than that calculated from the change in thickness. This difference was believed to be due to variations in the actual burning surface area attributable to burning along the edges, and to the starting and stopping transient effects.

The results obtained in the tube burner studies agreed well with expectations insofar as burning rate, pressure, and mass flux relationships were concerned. Fig. 18 is a plot of normalized burning rates showing a comparison of data from this investigation with that published previously.

/19/

Burning rates in the slab burner were generally much lower than for corresponding pressures and oxidizer flux rates in the tubular grain. The heat transfer dependence of the burning rate leads to the expectation that the presence of cold, heat-conducting walls in the slab burner would reduce the regression rate by reducing the heat transferred to the fuel surface.



In the early tests some difficulty was encountered in preventing burning of the slab on the bottom surface. This problem was eliminated by placing a layer of 1/64-inch gasket material beneath and along the edges of the slab and installing a brass or sheet steel fairing at the leading edge. (Fig. 19) This procedure provided the tight seal necessary to prevent oxidizer from flowing beneath the grain, but created serious problems in the measurement of heat flux. In the final configuration, the grains were sealed with General Electronics room temperature vulcanizing silicon rubber compound and no gaskets or fairings were used.

The formation of a char layer on the fuel grain surface under certain conditions of oxidizer mass flux and chamber pressure has been reported in the literature. [18,19] This phenomena occurs under conditions of low gas velocity in the chamber, and there is an evident link between burning rates at chamber pressures above five atmospheres and char formation. In this investigation the regimes conducive to char formation were intentionally avoided, because of the adverse effect of soot deposits on the viewing window of the resistance thermometers. Observations indicate, however, that the conclusions drawn by Lousma with regard to char formation and unsteady combustion in the tube burner apply as well to the slab grain configuration. The present instrumentation provides the capability to study the phenomenon of unsteady combustion (Fig. 17) and its connection with char formation, a worth while subject for future investigators.

#### Heat Transfer Measurement

The most critical requirement in the sequence of events involved in the heat transfer measurements was the rapid and complete exposure of the



gage face. This was expected to occur as the regressing fuel surface reached the location of the flux gage probe recess. This exposure must occur in the time span of a few milliseconds for the thin film to properly represent the surface of a semi-infinite solid in the theory. In the early phases of the investigation, evidence accrued to indicate that the gage face was not being rapidly exposed. This evidence first manifested itself in the form of a continuous curvature in the temperature trace, that is, there was no indication of step input in heat transfer to the gage. (Fig. 20)

The second indication that gage exposure was not sufficiently rapid was the evidence of incomplete exposure after shutdown. Evidently the exposure began with "burn through" at some point in the gage face area. This initial "burn through" was followed by progressive, but not rapid, expansion of the exposed area. Several slabs with incomplete aperture opening are shown in Fig. 21. The fact that this process occurred over a period of more than a few milliseconds was amply demonstrated by the fact that the investigator could shut down the apparatus between the beginning of exposure and complete opening of the aperture. This phenomenon not only upsets the application of the theory, but it also prevented obtaining any indication of radiation heat transfer to the film of the gage. As the aperture slowly opened, combustion products deposited on the exposed glass and obscured the "view" of the platinum element. The absorptivity of a lamp black film is of the order of 98%, so that a small deposit of soot was sufficient to obscure the gage. Examples of this deposition of combustion products on the probe face are shown in Fig. 22.

Several approaches were made to elimination of this problem of slow exposure. The most efficacious of these was a large increase in burning rate obtained by using much higher oxidizer flow rates. Secondly, a layer of heavy aluminum foil was placed over the face of the gage to obscure the gage until released by complete opening of the aperture.

The early work was done at low pressure (three atmospheres). It was evident, however, after a few trials, that the gage temperature-increases being measured were not of sufficient magnitude to allow confident reduction to a heat transfer value. Hence it was also necessary to take advantage of the pressure dependency of the radiation component by increasing the chamber pressure. Experiments which yielded useful gage temperature histories were at chamber pressures of over nine atmospheres. The values of radiant heat transfer to the fuel surface as measured in this investigation appear in Table II and Figures 23 and 24.

Improved flux gage sensitivity can be obtained by coating the face of the resistance thermometer with lampblack. This technique increases the uniformity of absorption over the infrared bandwidth. Care must be exercised that the  $\text{MgF}_2$  coating is intact since the platinum must be insulated electrically from the carbon. By this means it might be possible to obtain data in regimes of low values of radiation with the present instrumentation.

One of the setbacks which delayed data collection occurred when the brass fairing at the leading edge of the grain burned, sending large, hot metallic oxide particles downstream. The radiation from these particles was quite high and unsteady, so that its presence was easily seen in the

gage temperature history. (Fig. 25) Use of a steel fairing caused additional trouble when the molten metal oxide accumulated in the aft end of the burner and melted a small portion of the aft closure assembly. The damaged fairings and aft closure are shown in Fig. 26. Damage was not serious, but the use of metal fairings was discontinued.

The flux gages and the phenolic holders withstood the rigors of the environment remarkably well. Only one of the six gages was destroyed during the course of the investigations. This occurred when the gage was exposed through the burner wall opposite the fuel slab. Exposure in this highly oxidizing atmosphere burned the phenolic laminate very rapidly, released the protecting window and consumed the platinum film as is shown in Fig. 27. Total burning time for that firing was under three seconds.

During the early stages of the investigation (at low burning rates) the first probe used survived nearly a dozen runs before it was taken out of service to replace the glass and repair the phenolic holder. At high burning rates the damage to the probe during each run was more severe. The metal oxides from the destruction of the leading edge fairings damaged the glass, as did the aluminum oxide deposits from the metalized propellants. Under these conditions the probes often survived only one firing. Reconstruction of a damaged probe required about four man hours on the part of a technician and 48 hours for the curing of the epoxy cements used. Collection of data thus proceeded at an agonizingly slow pace, averaging less than one test per day.

The production rate in the tube burner was even slower because of the additional requirement for a 24-hour curing time for the epoxy which

bonded the gage into the grain wall. Essentially, because of the extensive effort expended in the slab burner tests, the tube burner test series was not completed.

The most reasonable solution to the problem of preservation of the heat sensor probes would be to manufacture them from a ceramic material and provide for expeditious replacement of the viewing window. Design and construction of the thin film gages themselves specifically for this application could reduce the size of the probe and help to eliminate the severe restriction on the number of gages available that was imposed on this investigation.

In analyzing the limited data obtained in this investigation, it is reasonable to examine Eq. (3) again.

$$\dot{Q}_r = \sigma \epsilon_w T_r^4 \left[ 1 - e^{-\alpha n z} \right] \quad (3)$$

In this equation  $\alpha$ ,  $n$ , and  $z$  are essentially unknown. The emissivity of the wall ( $\epsilon_w$ ) is bounded ( $0 \leq \epsilon_w \leq 1$ ) and may be reasonably expected to be approximately 0.90. The flame temperature ( $T_r$ ) can be obtained theoretically and has been verified experimentally so that reasonable values of  $T_r$  can be introduced. If  $\epsilon_w$  and  $T_r$  are considered to be established, then a measured value of  $\dot{Q}_r$  will produce a value of  $\alpha n z$  applicable to a particular fuel-oxidizer system. Initially this value must be considered to be restricted in applicability to the chamber conditions under which it was obtained. With the accumulation



of more data it would, hopefully, be possible to establish  $\alpha n z$  as a function of geometry, pressure, and oxidizer flux rates. The authors of the theory leading to Eq. (1) have supposed that  $\alpha$  is a constant for a particular fuel-oxidizer combination. The pressure dependence of the radiation heat transfer term then should appear in  $n$  as has also been assumed. The optical path length ( $z$ ) may vary with position in the fuel grain ( $L/D$ ), but should, at a given location, be constant for a particular geometry and propellant combination.

An initial analysis of the data at hand must be satisfied with simply the establishment of the value of the exponent as a lumped parameter for the geometry and systems studied. A more detailed analysis of the individual parameters must await more extensive studies of the variation of  $\dot{Q}_r$  with pressure, mass flow rates, and internal geometry. Inverting Eq. (3) yields

$$\alpha n z = -1/n \left[ 1 - \frac{\dot{Q}_r}{\sigma \epsilon_w T_r^4} \right] \quad (7)$$

Solutions to Eq. (7) require measured values of  $\dot{Q}_r$ , an assumption of a value for  $\epsilon_w$ , and a value for  $T_r$ . It is convenient to allow  $T_r$  to vary over a reasonable range and to plot  $\alpha n z$  in terms of  $\dot{Q}_r$  with  $T_r$  as a parameter. Such a plot appears in Fig. 28. Entering this chart with data from Table II yields the following values of  $\alpha n z$  for the propellant systems studied:



Propellant System	P	T <sub>r</sub>	$\alpha_{nz}$
Polystyrene Oxygen	9.85	3725	0.066
	10.55	3725	0.079
	12.55	3725	0.116
Plexiglas with 20% Al	9.84	4000	0.087

These values are based on a very limited amount of data. Future studies should expand the range of pressures and oxidizer flow rates investigated. The slab burner should also facilitate the direct measurement of flame temperatures by use of high temperature thermocouple technology and dilute oxidizer mixtures. The combination of such measurements with the measured values of radiant heat flux should provide an excellent background for future analysis of the contribution of radiant heat transfer to the hybrid rocket combustion mechanism.

Examination of figures 23 and 24 shows that the radiant heat transfer to the fuel surface increases with pressure and decreases with oxidizer flow rate. The increase with pressure was anticipated and is explained principally by the effect of pressure on the concentration of radiating particles, that is an increase in  $n$  in the exponential term of Eq. (3). The decrease in  $\dot{Q}_r$  with increased  $G_o$  was anticipated on the basis of limited published experimental evidence. [7] No explanation for this is offered at this time.

During one test the protecting window was carried away from the probe just prior to shutdown. The test involved a black polystyrene grain in the slab burner. This accident proved fortuitous in that it provided a

trial test of the feasibility of obtaining total heat transfer measurements with the thin film gages. Tests of this nature have been proposed, but because of the limitation on the number of gages (and the probability of damage) it was not anticipated that they would be conducted until all the radiation measurements were complete or until local manufacture of gages is possible. The value of the total heat transfer for this single test was

$$\dot{Q}_{total} = 91.16 \text{ BTU/ft}^2\text{-sec}$$

Subtracting the radiation measurement obtained 0.78 sec. earlier in the same test yields

$$\dot{Q}_c = 82.01 \text{ BTU/ft}^2\text{-sec}$$

which indicates that only 11.15 percent of the heat transfer was due to radiation. Conditions in the chamber were:

$$P = 12.55 \text{ atm.}$$

$$G_o = 0.127 \text{ lbm/in}^2\text{-sec}$$

Using these values of  $Q_r$  and  $Q_c$  and assuming  $h_{veff} = 500 \text{ cal/gm}$  the burning rate given by Eq. (1) is 0.0165 in/sec. The measured burning rate from Table II for this run was 0.017 in/sec. On the basis of this single exposure of the gage (which it survived without damage), the technique appears feasible. Such tests would be an outstanding adjunct to the measurement of radiation heat transfer, providing a nearly complete experimental description of the character of heat transfer to the fuel surface.

## 5. Conclusions.

The hybrid rocket test apparatus performs satisfactorily in its present configuration. Improvements to the supply, control, and instrumentation made during this investigation increased the usefulness of the apparatus and markedly enhanced the safety of the operator. The addition of a two-dimensional slab burner provides versatility in the type of studies that can be conducted. The performance of the slab burner was satisfactory and with minor modifications this equipment can provide for a wide range of research endeavors.

The collection of burning rate data in the slab burner using the light sensor technique was not realized. Modification to the burner is necessary if this method is required in future studies.

Measurement of radiant heat transfer to the regressing fuel surface in the hybrid rocket using thin film resistance thermometers is conceptually sound. Improvements in gage sensitivity with carbon black coating on top of the magnesium fluoride which protects the platinum film should enhance the ability to measure low levels of radiation. Ceramic materials and reduced gage dimensions would provide additional probe life and increase the rate of data collection.

The problem of obtaining gage face exposure in the required few milliseconds was not solved in the tubular grain in this investigation. Hence, the applicability of the technique to the tubular geometry remains to be demonstrated.

The values of radiant energy transfer to the fuel measured in this investigation agree reasonably with published calculations and estimates,

although the data reported here is not considered to be conclusive. There remains considerable requirement for parametric study before proceeding with the establishment of a relationship for the lumped parameter with pressure, flow, rates, geometry and the fuel-oxidizer combination.

On the basis of a single experiment it appears that the measurement of total heat transfer to the fuel surface with thin film resistance thermometer is a feasible endeavor.

## 6. Suggestions for Further Investigations

The existing hybrid rocket test apparatus is versatile and lends itself to a variety of experimental endeavors. The following paragraphs contain a few suggested applications, but are not intended to encompass the entire scope of possibilities.

The present investigation should be continued and expanded. The technical feasibility has been amply demonstrated, the equipment is available and adequate, and the fuel is available. An experimental description of the heat transfer to the solid fuel surface in the hybrid rocket in terms of chamber pressure and mass-flow-rate of oxidizer should be attainable. Both total and radiative heat flux values should be measured.

Local capability to manufacture thin film resistance thermometers should be developed. These devices are quite expensive to purchase and, in this application, must be considered to be somewhat expendable. Hence, for any extensive investigation, an adequate supply of gages should be assured by local manufacture. Dual element gages are described in Ref. 11 which have the capability of simultaneous measurement of total and



radiative heat flux. This gage construction would be ideal for the proposed studies.

Two windows of Corning No. 7940 clear fused silica have been purchased for installation in the side closures of the slab burner. These two-inch diameter, one-half inch thick windows were pitch polished flat to one wave length and were obtained for use in photographic studies of the flame zone on the slab. An Eastman Kodak 16mm high speed framing camera, capable of up to 3000 frames per second, is available for photographic investigations.

Investigation of the relationship between char formation and regression rates in certain fuels should be continued as suggested in Ref. 19.

The control system for the hybrid rocket test table should be modified to include an automatic sequencing capability. This can be done at nominal cost and would free the operator from mechanical manipulation of the operating sequences.



## BIBLIOGRAPHY

1. Vidal, R. J. Model Instrumentation Techniques for Heat Transfer and Force Measurements in a Hypersonic Shock Tunnel. Cornell Aeronautical Laboratory Report AD-917-A-1; WADC TN 56315 AD97238. February 1956.
2. Skinner, G. T. Analog Network to Convert Surface Temperature to Heat Flux. Cornell Aeronautical Laboratory. Report CAL-100. February 1960.
3. Lee, L. W. et al. Feasibility of Hybrid Rocket Systems. U. S. Army Rocket and Guided Missile Agency. ARGMA TR2E3R. 13 February 1961. (C)
4. Barber, H. et al. Research and Development of Hybrid Propellants. Aerojet General Corporation. Quarterly Report 0532-01-1. October 1961. (C)
5. Solomon, S. E. et al. Hybrid Rocket Engine Feasibility Program. Aerojet General Corporation. Feasibility Report 0382-04F. 9 April 1962. (C)
6. Iwanciow, B. L. et al. Investigation of Fundamental Phenomena in Hybrid Propulsion. United Technology Center. Quarterly Technical Summary Report, UTC 2097-QT3. April 1963. (C)
7. Iwanciow, B. L. et al. Investigation of Fundamental Phenomena in Hybrid Propulsion. United Technology Center. Quarterly Technical Summary Report; UTC 2051-QT1. September 1963. (C)
8. Taylor, R. L. et al. Investigation of Fundamental Phenomena in Hybrid Propulsion. United Technology Center. Quarterly Progress Report; UTC 2097-QPR1. September 1963. (C)
9. Iwanciow, B. L. et al. Investigation of Fundamental Phenomena in Hybrid Propulsion. United Technology Center. Quarterly Technical Summary Report; UTC 2051-QT2. December 1963. (C)
10. Marxman, G. A. et al. Fundamentals of Hybrid Boundary Layer Combustion, Heterogeneous Combustion. Progress in Astronautics and Aeronautics. Academic Press Inc., v. 15, 1963.
11. Bogdan, Leonard. Measurement of Radiative Heat Transfer With Thin-Film Resistance Thermometers. National Aeronautics and Space Administration. Contract Report 27. March 1964.

12. Iwanciw, B. L. et al. Investigation of Fundamental Phenomena in Hybrid Propulsion. United Technology Center. Quarterly Technical Summary Report; UTC 2051-QT3. March 1964. (C)
13. Bogdan, Leonard. High Temperature, Thin Film Resistance Thermometers for Heat Transfer Measurement. National Aeronautics and Space Administration. Contractors Report CR 26. April 1964.
14. Thomas, G. M. and Menard, W. A. Total Radiation Heat Transfer Gage for Hypervelocity Shock Tube Experiments. Jet Propulsion Laboratory. Technical Report No. 32-636. 1 August 1964.
15. Lawrence, R. W. et al. Investigation of Advanced Hybrid Propellants. Aerojet General Corporation. AGCR 0722-01-1. January 1965. (C)
16. Smoot, L. D. and Price, C. F. Regression Rate Mechanisms of Non-metallized Hybrid Fuel Systems. American Institute of Astronautics and Aeronautics Paper 65-56, Second Aerospace Sciences Meeting. New York, January 1965.
17. Smoot, L. D. et al. Regression Rate Mechanisms of Metallized Hybrid Fuel Systems. American Institute of Astronautics and Aeronautics, Sixth Solid Propellant Combustion Conference, Washington, D. C. 1-3 February 1965. (C)
18. Marxman, G. A. and Wooldridge, C. E. Research on the Combustion Mechanism of Hybrid Rockets. 25th Meeting of the Combustion and Propulsion Panel, AGARD, NATO, La Jolla, California. 22-23 April 1965.
19. Lousma, J. R. A Parametric Burning Rate Study of the Polystyrene-Oxygen Hybrid Fuel System. Aeronautical Engineering Department, U. S. Naval Postgraduate School, Monterey, California. May 1965. (C)
20. Reece, J. W. and Theoclitus, G. A New Technique for Measuring Thermal Radiation. 1965 Aerospace Conference and Exhibit, Houston, Texas. June 1965.
21. Paddock, D. A. and Hardy, R. G. A New Thermal Radiative Flux Gage. Instrument Society of America, 20th Annual I. S. A. Conference and Exhibit, Los Angeles, California. October 1965.

TABLE I

## HYBRID ROCKET TEST DATA

U. S. Naval Postgraduate School  
Monterey, California

Henry L. Searle  
Capt., USMC

Test No. \_\_\_\_\_ Date: \_\_\_\_\_

Atm. Conditions:  $P_a =$  \_\_\_\_\_ in Hg = \_\_\_\_\_ psi  $T_a =$  \_\_\_\_\_  $^{\circ}\text{F}$

Fuel Grain No. \_\_\_\_\_

Pressures:

Fuel Type \_\_\_\_\_

$P_o =$  \_\_\_\_\_ psig = \_\_\_\_\_ psia

Grain Size:

$P_c =$  \_\_\_\_\_ psig = \_\_\_\_\_ psia

Length:  $L =$  \_\_\_\_\_ in

$\dot{m}_o =$  \_\_\_\_\_ lbm/sec

InsideD:  $D_o =$  \_\_\_\_\_ in  $D_f =$  \_\_\_\_\_ in  $\Delta D =$  \_\_\_\_\_ in

Width:  $b =$  \_\_\_\_\_ in

Thickness:  $t_s =$  \_\_\_\_\_ in  $t_{sf} =$  \_\_\_\_\_ in  $\Delta t_s =$  \_\_\_\_\_ in

Weight:  $W_o =$  \_\_\_\_\_ gm  $W_f =$  \_\_\_\_\_ gm  $\Delta W =$  \_\_\_\_\_ gm

Flux Gage:

Burn Times:

Depth:  $d_f =$  \_\_\_\_\_ in

$t_b =$  \_\_\_\_\_ sec

$L/D =$  \_\_\_\_\_

$\Delta t =$  \_\_\_\_\_ sec

Light Probes:

Burning Rates:

$d_1 =$  \_\_\_\_\_ in

$r = \Delta d / \Delta t =$  \_\_\_\_\_ in/sec

$d_2 =$  \_\_\_\_\_ in

$r = \Delta t_s / t_b =$  \_\_\_\_\_ in/sec

$\Delta d =$  \_\_\_\_\_ in

$r = \Delta W / \rho A t_b =$  \_\_\_\_\_ in/sec

$L/D =$  \_\_\_\_\_

$P = P_c / P_a =$  \_\_\_\_\_ atm

Choke Diam:  $D_c =$  \_\_\_\_\_ in

$G_o =$  \_\_\_\_\_ lbm/in<sup>2</sup>sec

Throat Diam:  $D_t =$  \_\_\_\_\_ in

Gage Sensitivity: \_\_\_\_\_  $^{\circ}\text{F/in}$

Flux Gage No. \_\_\_\_\_

$R_{og} =$  \_\_\_\_\_ ohms  $T_{og} =$  \_\_\_\_\_  $^{\circ}\text{F}$

REMARKS:

TABLE II

## SUMMARY OF EXPERIMENTAL RESULTS

## Tube Burner Data

Run No.	Fuel*	P atm	$t_b$ sec	$r = \frac{\Delta t_s}{\Delta t_b}$ $\frac{\text{in}}{\text{sec}}$	r from $\Delta w$ $\frac{\text{in}}{\text{sec}}$	$G_o^\circ$ $\frac{\text{lbm}}{\text{in}^2\text{-sec}}$
T-301	BPS	3.38	5.95	0.0163		0.046
T-203	CPS	11.20	4.83	0.0295	0.0225	0.189
T-204	CPS	10.90	2.74	0.0305	0.0332	0.189
T-205	BPS	11.20	3.07	0.0282		0.178
T-206	BPS	11.20	2.94		0.0326	0.178
T-207	BPS	13.25	2.44	0.0295	0.0360	0.198
T-208	BPS	13.95	4.43	0.0177	0.0242	
T-209	BPS	9.52	6.55	0.0173	0.0185	0.185
T-210	BPS	9.52	7.53	0.0220	0.0227	0.200
T-211	BPS	9.80	7.40	0.0225	0.0234	0.200

## Slab Burner Data

Run No.	Fuel*	P atm	$t_b$ sec	$r = \frac{\Delta t_s}{t_b}$ $\frac{\text{in}}{\text{sec}}$	$r = \frac{\Delta w}{At_b \rho}$ $\frac{\text{in}}{\text{sec}}$	$G_o^\circ$ $\frac{\text{lbm}}{\text{in}^2\text{-sec}}$	$Q_r$ $\frac{\text{BTU}}{\text{ft}^2\text{-sec}}$
S-101	PMM	3.04	4.54	0.010	0.0031	0.015	
S-102	PMM	3.69	6.30	0.006	0.0088	0.024	
S-103	CPS	4.71	5.41	0.009	0.0104	0.049	
S-104	BPS	3.03	5.64	0.006	0.0058	0.025	
S-105	BPS	3.17	8.65	0.004	0.0058	0.024	
S-106	CPS	10.48	5.28	0.011	0.0144	0.065	
S-431	BPS	2.79	11.26	0.004	0.0042	0.019	
S-432	20A	3.18	11.64	0.003	0.0057	0.024	
S-201	BPS	2.36	8.42	0.006	0.0070	0.045	
S-205	CPS	2.72	2.94	0.013	0.0150	0.165	
S-206	BPS	2.36	3.72	0.012	0.0180	0.179	
S-213	20A	2.36	4.56	0.018	0.0150	0.166	
S-215	20A	12.82	2.83	0.019	0.0200	0.184	
S-216	20A	9.84	2.63	0.020	0.0200	0.183	9.24
S-217	BPS	12.55	3.52	0.017	0.0210	0.127	9.15
S-218	BPS	12.25	2.62	0.020	0.0240	0.171	
S-219	BPS	10.55	2.20	0.023	0.0240	0.156	7.08
S-220	BPS	9.85	2.55	0.022	0.0220	0.183	5.26
S-221	40A	9.55	3.75	0.018	0.0210	0.183	

\*CPS: Clear Polystyrene

BPS: Black Polystyrene

20A: Plexiglas with 20% Aluminum

40A: Plexiglas with 40% Aluminum

PMM: Plexiglas (Polymethylmethacrylate)

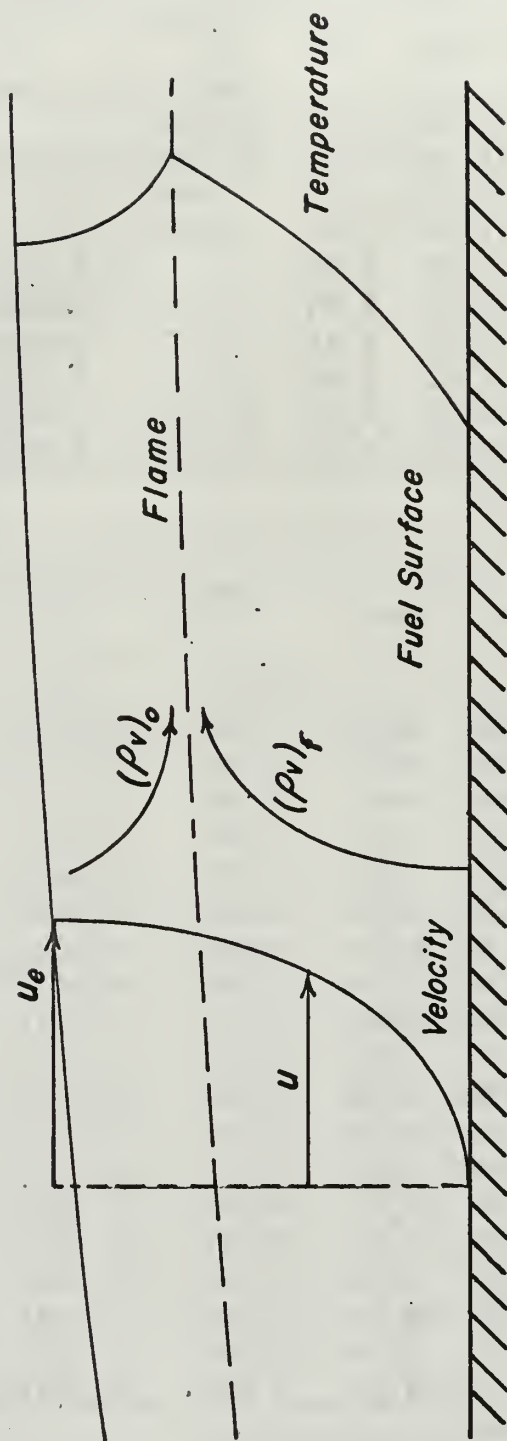


**Fig. 1**  
**Boundary Layer Combustion Model**



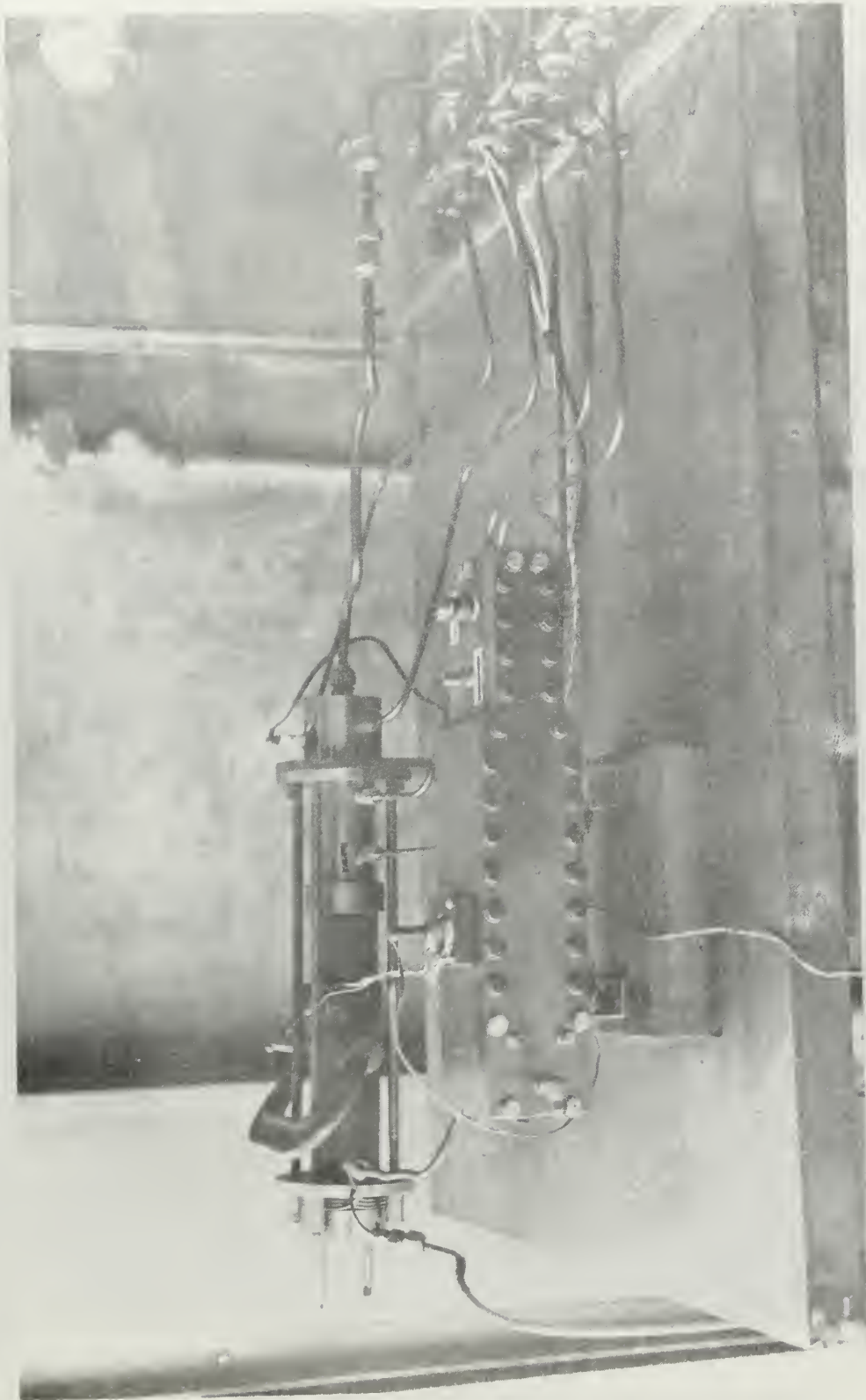


*Fig. 2*  
*Burner Assemblies*

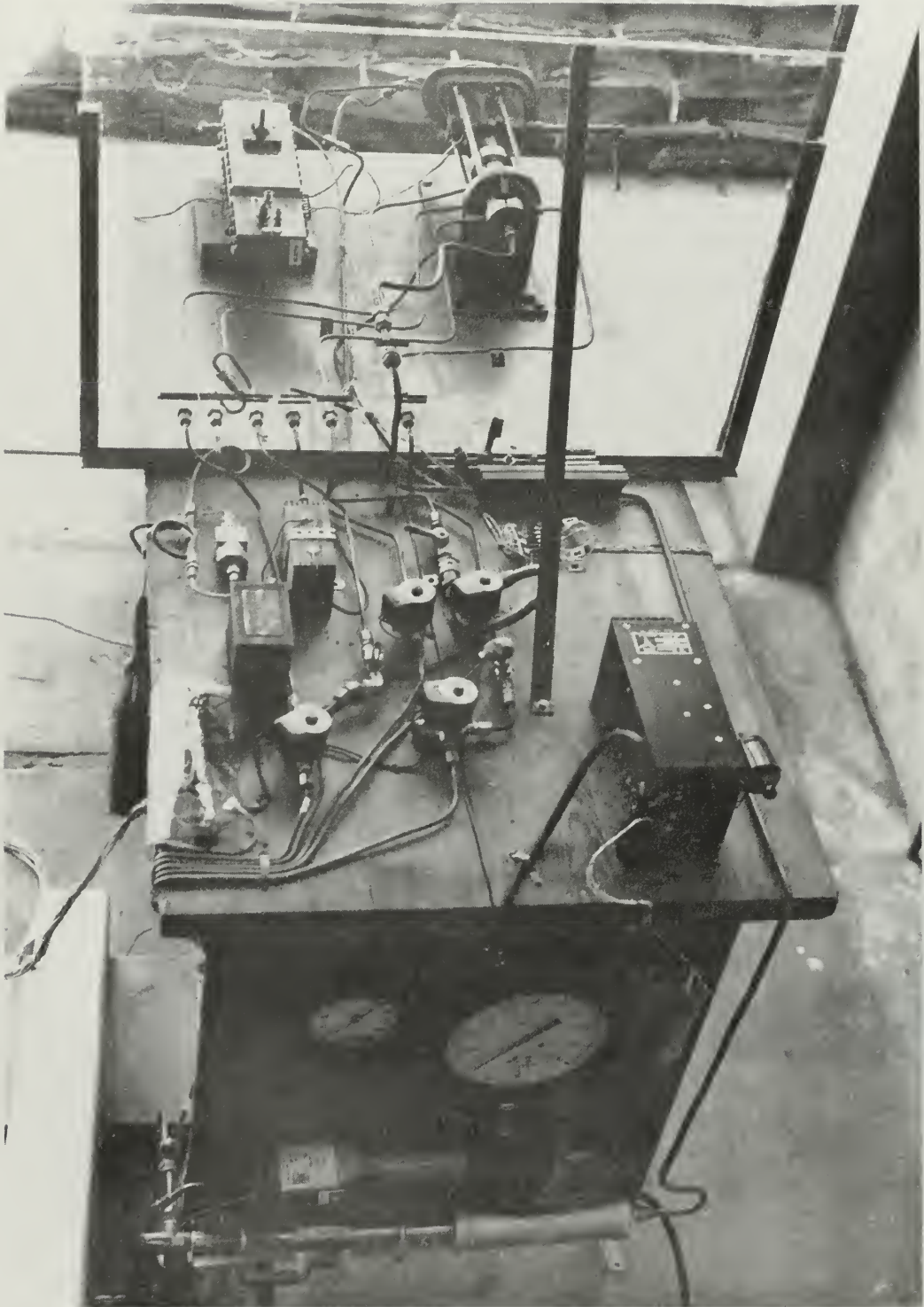


*Fig. 3*  
*Overall View of the Hybrid Rocket Test Table*

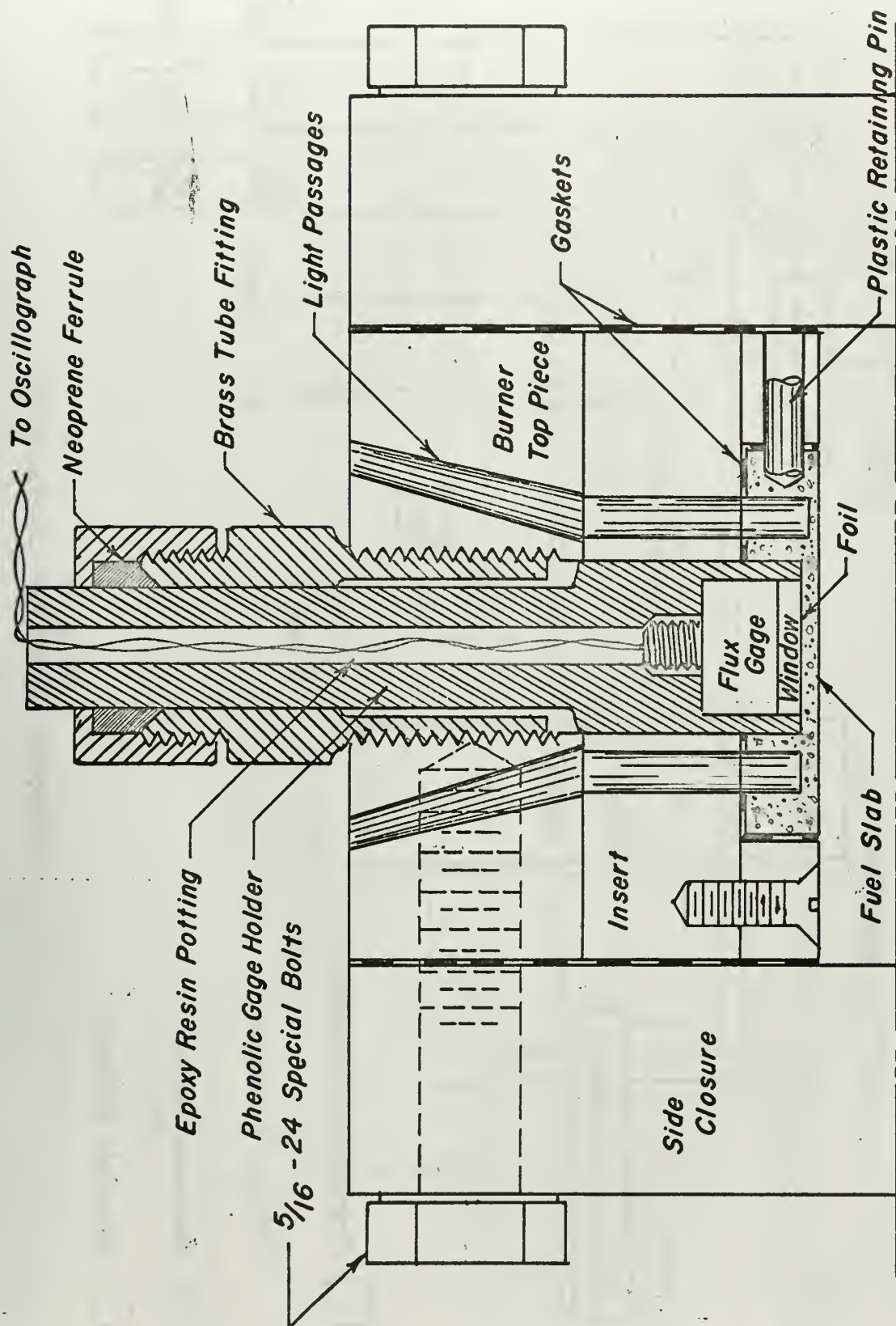


Fig. 4  
Cross Section of Slab Burner Showing Instrumentation Detail



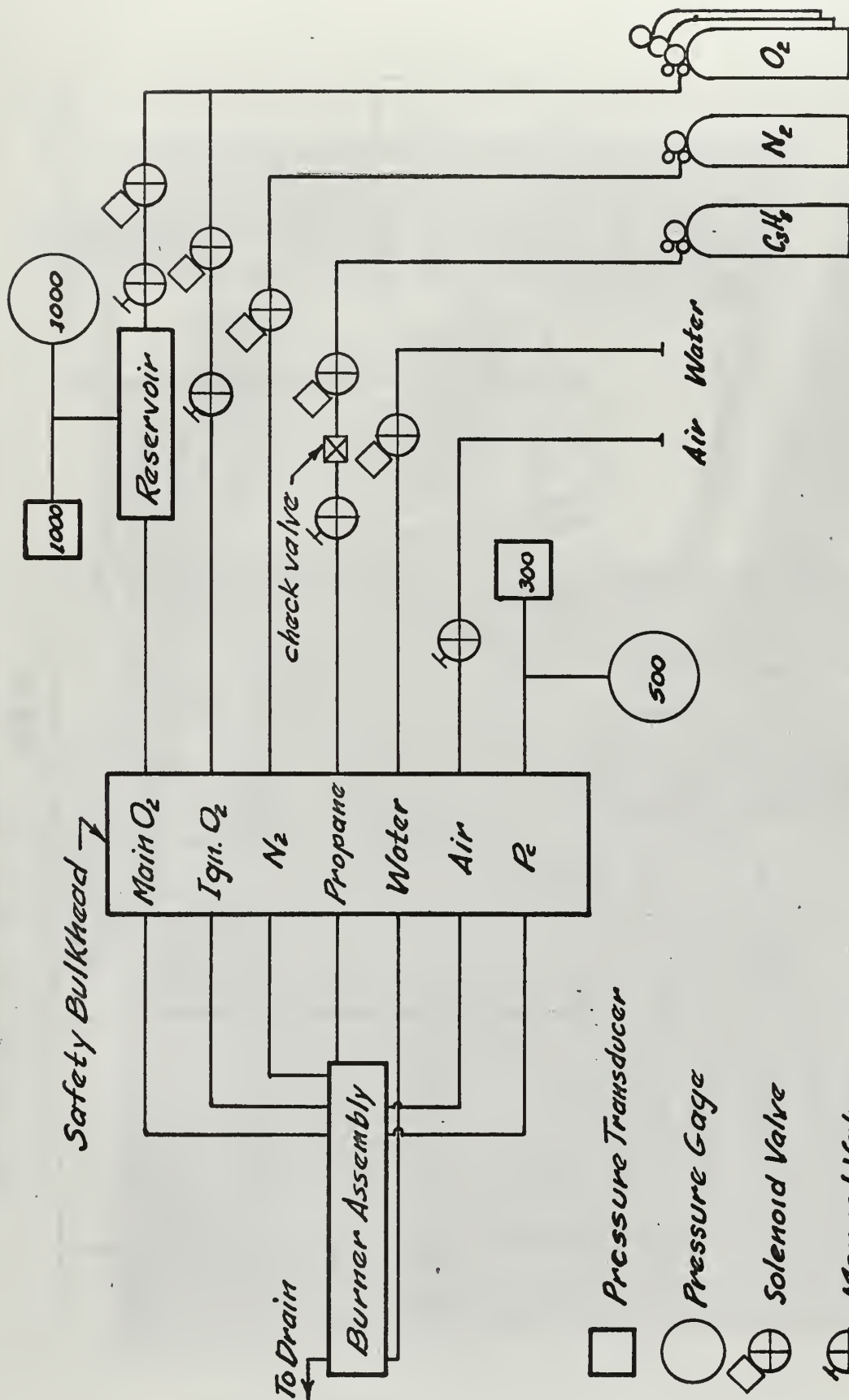


Fig. 5  
Supply System Schematic







Fig. 7  
Heat Sensor Component's



*Fig. 8*  
*Complete Heat Sensor Probes*

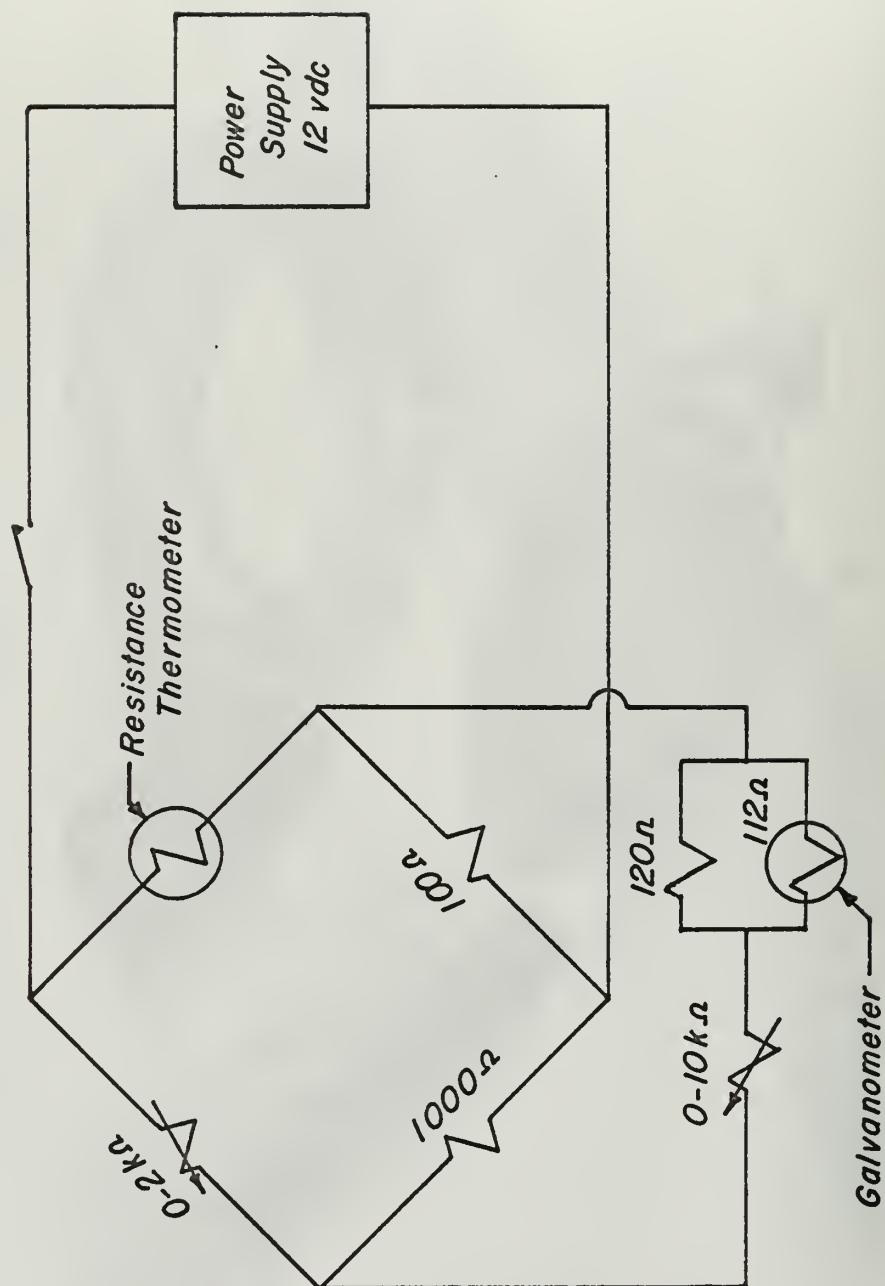
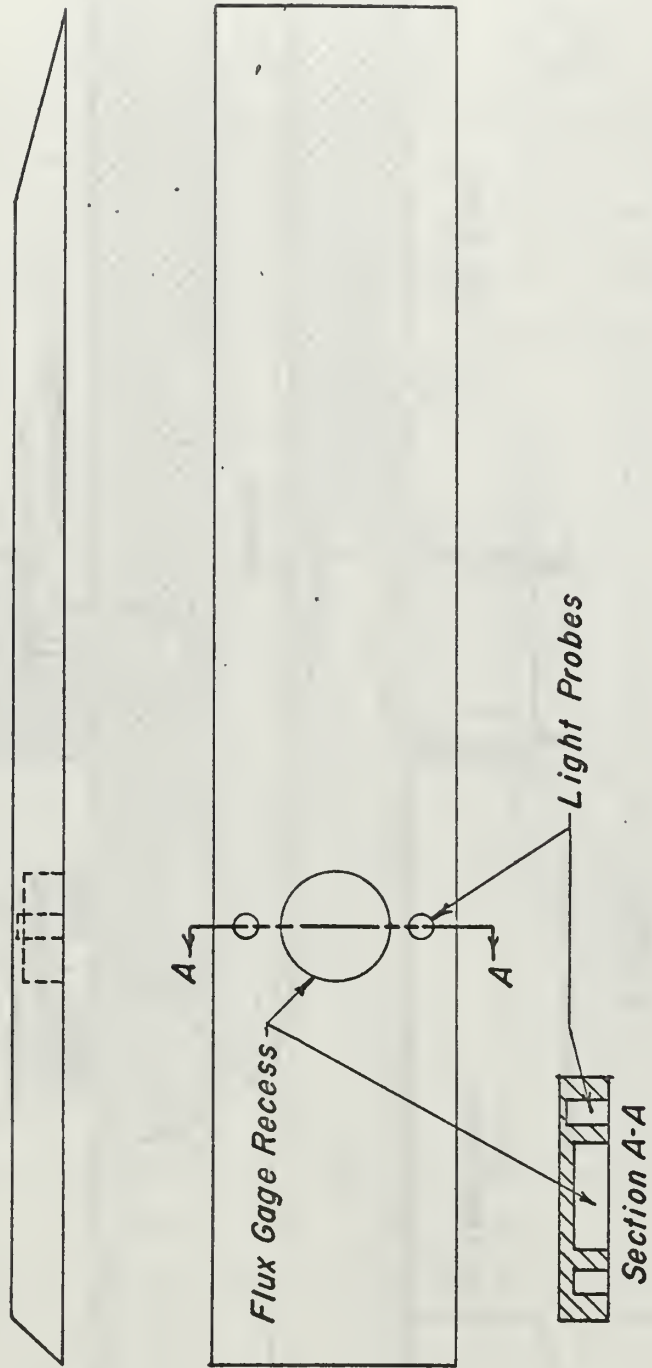


Fig. 9  
Flux Gage Bridge Circuit



*Fig.10*  
*Slab Grain Detail*

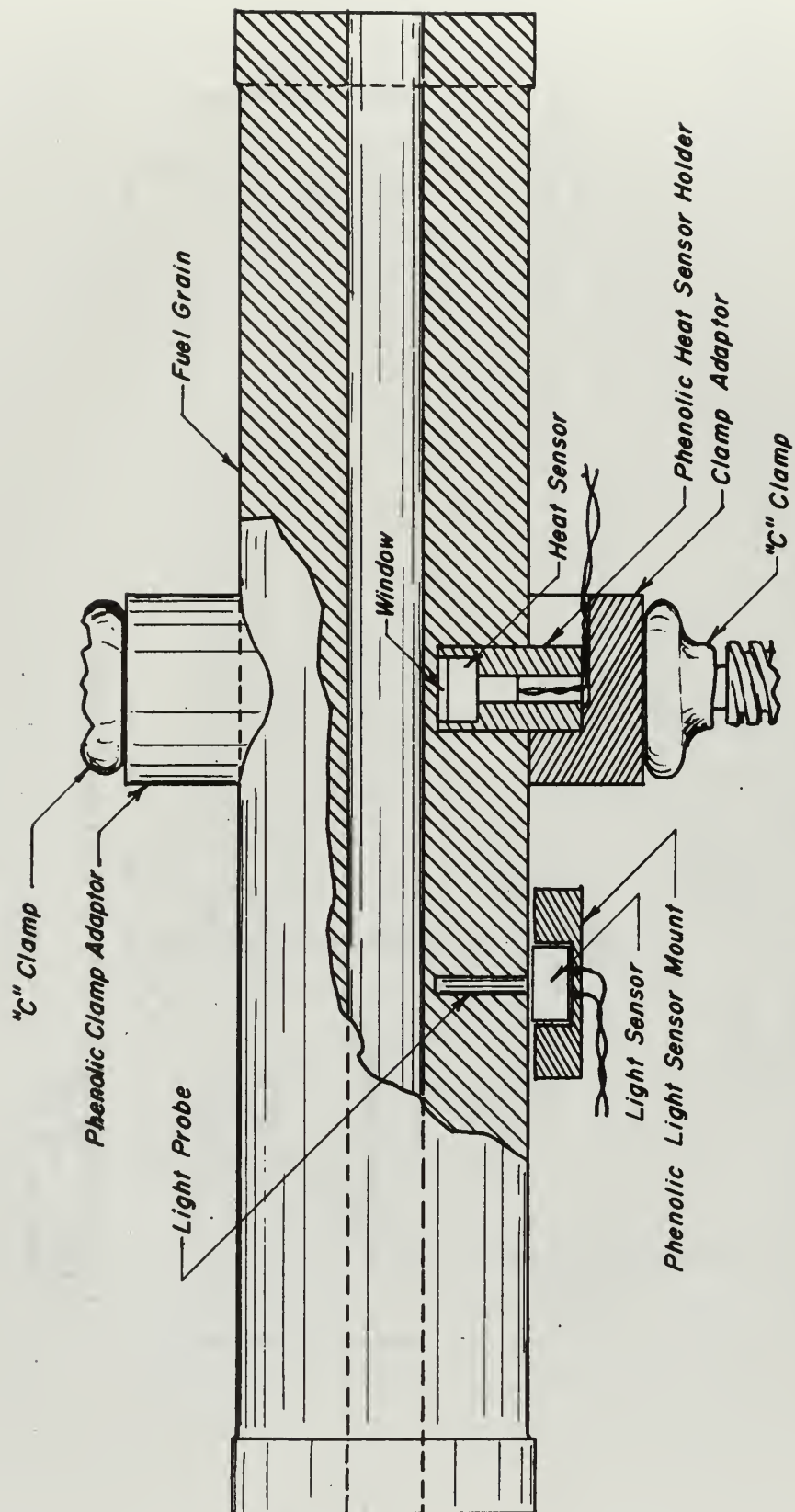


Fig. 11  
Tubular Grain Cross Section





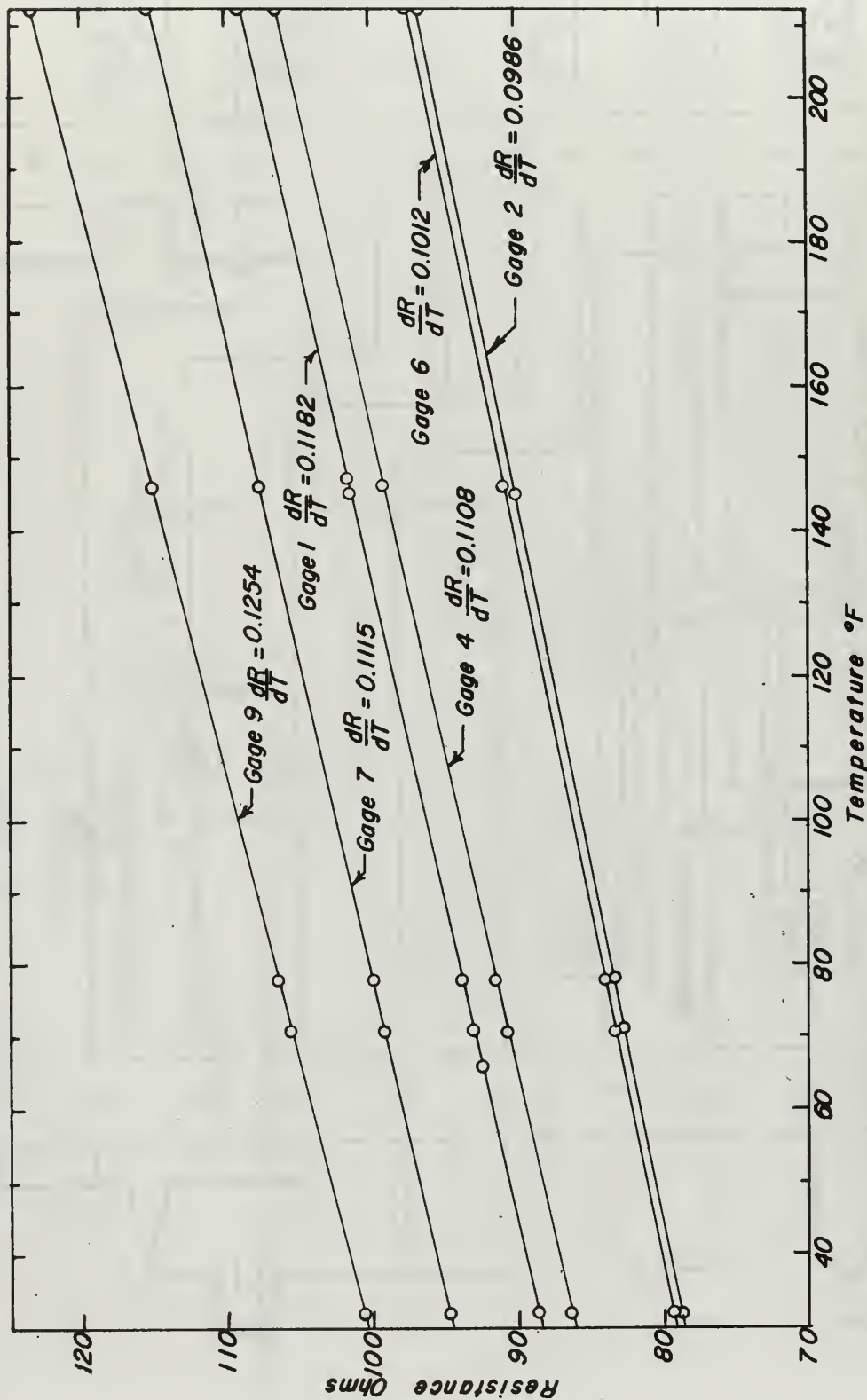
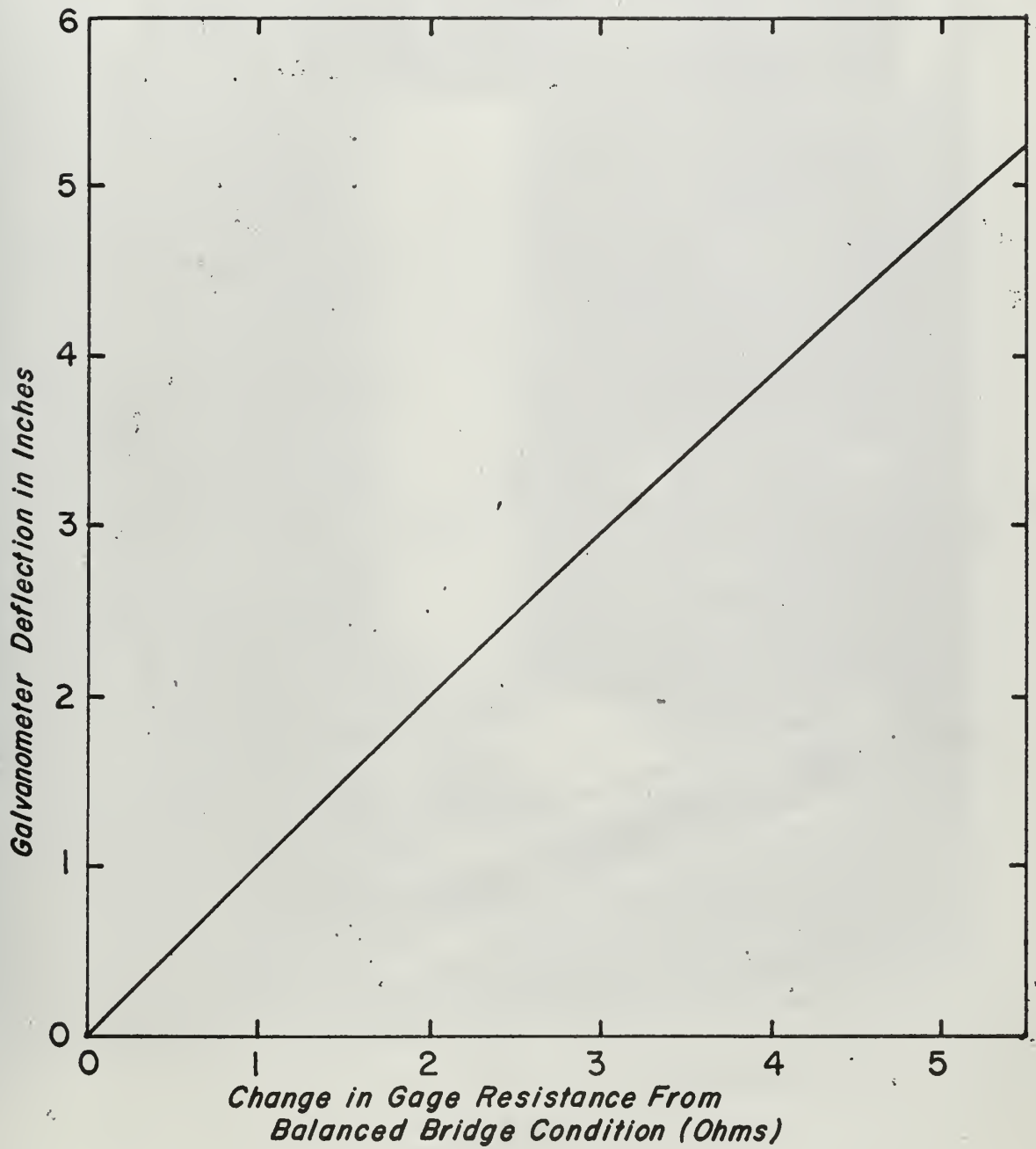
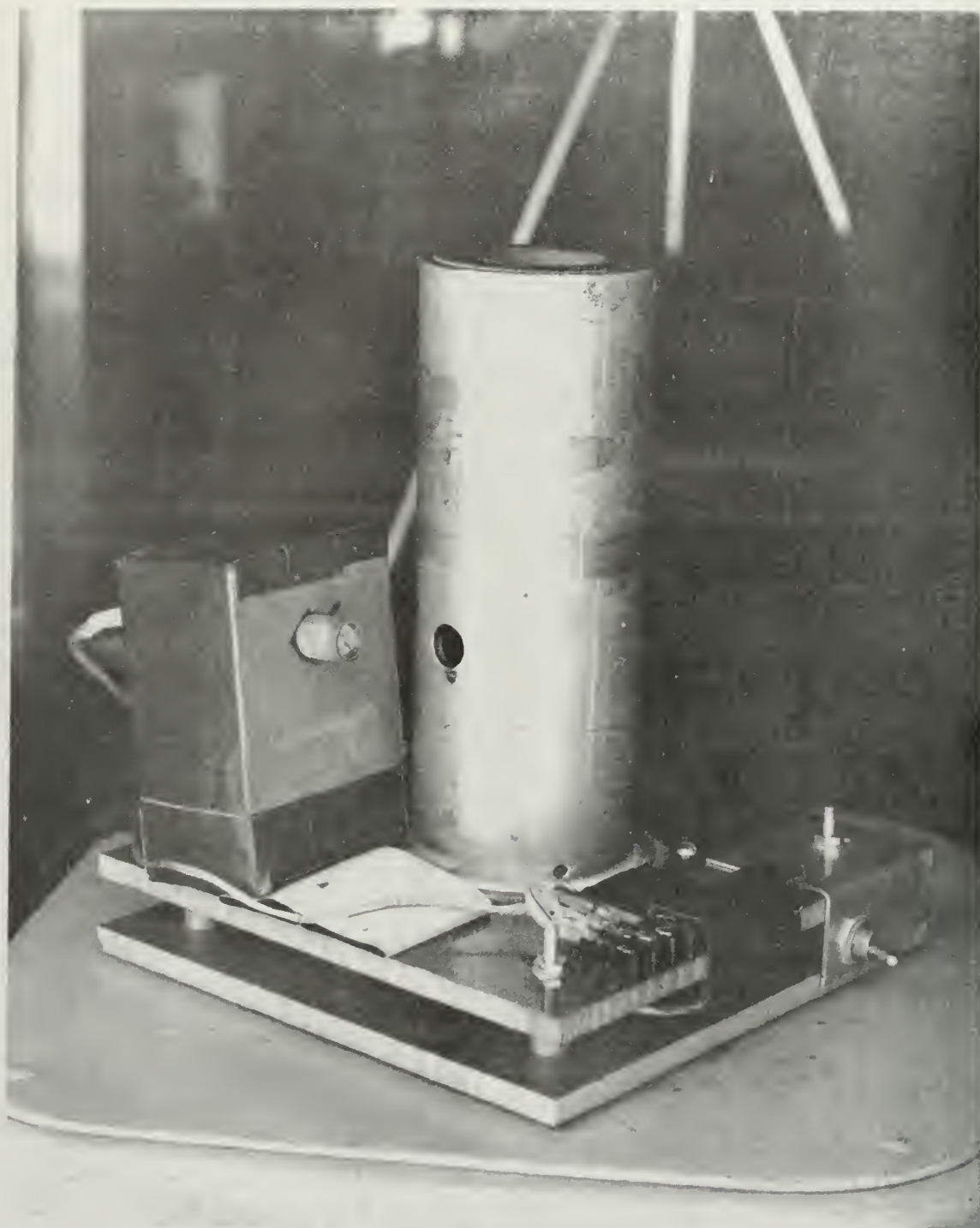


Fig. 13 Flux Gage Resistance-Temperature Characteristics



*Fig.14*  
*Galvanometer Sensitivity*



*Fig. 15*  
*Radiant Heat Source*

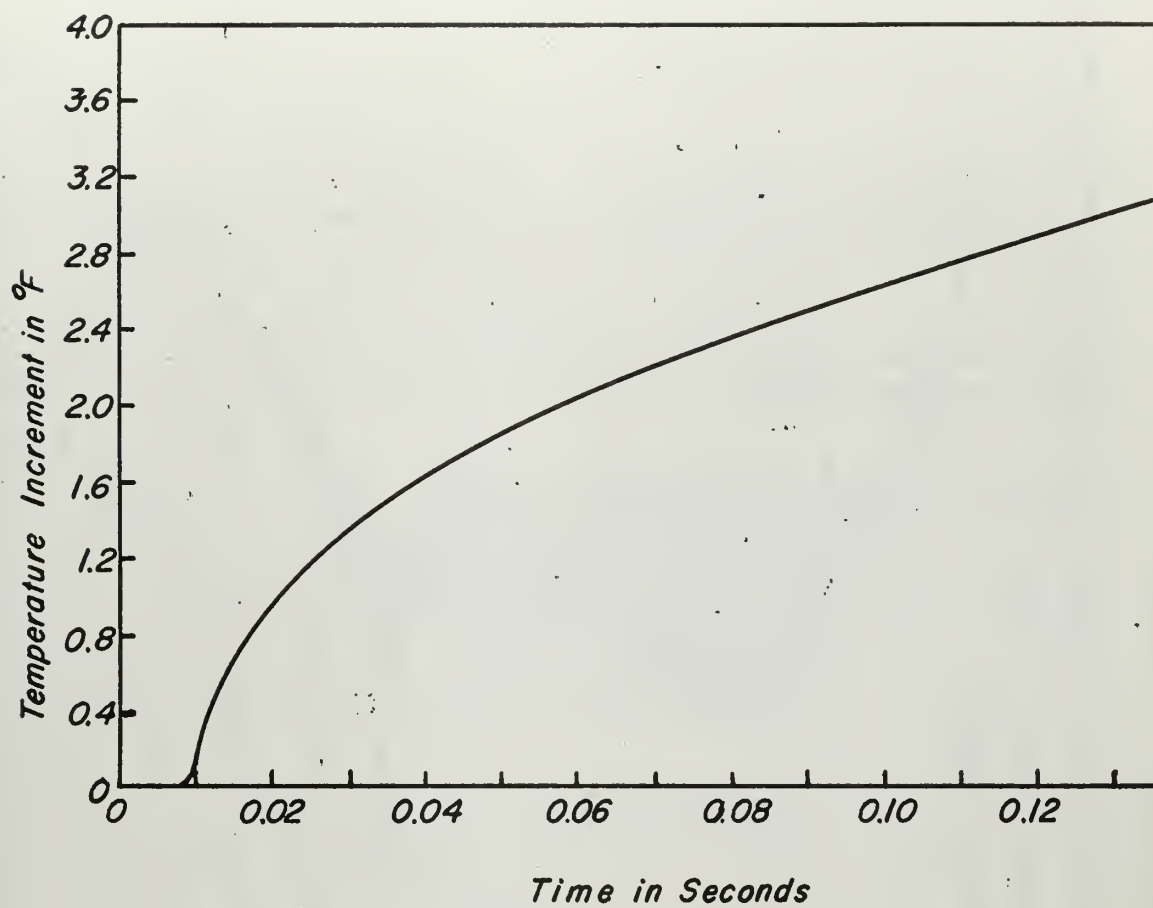


*Fig. 16*

*Gage Temperature History From Heat Source Input*



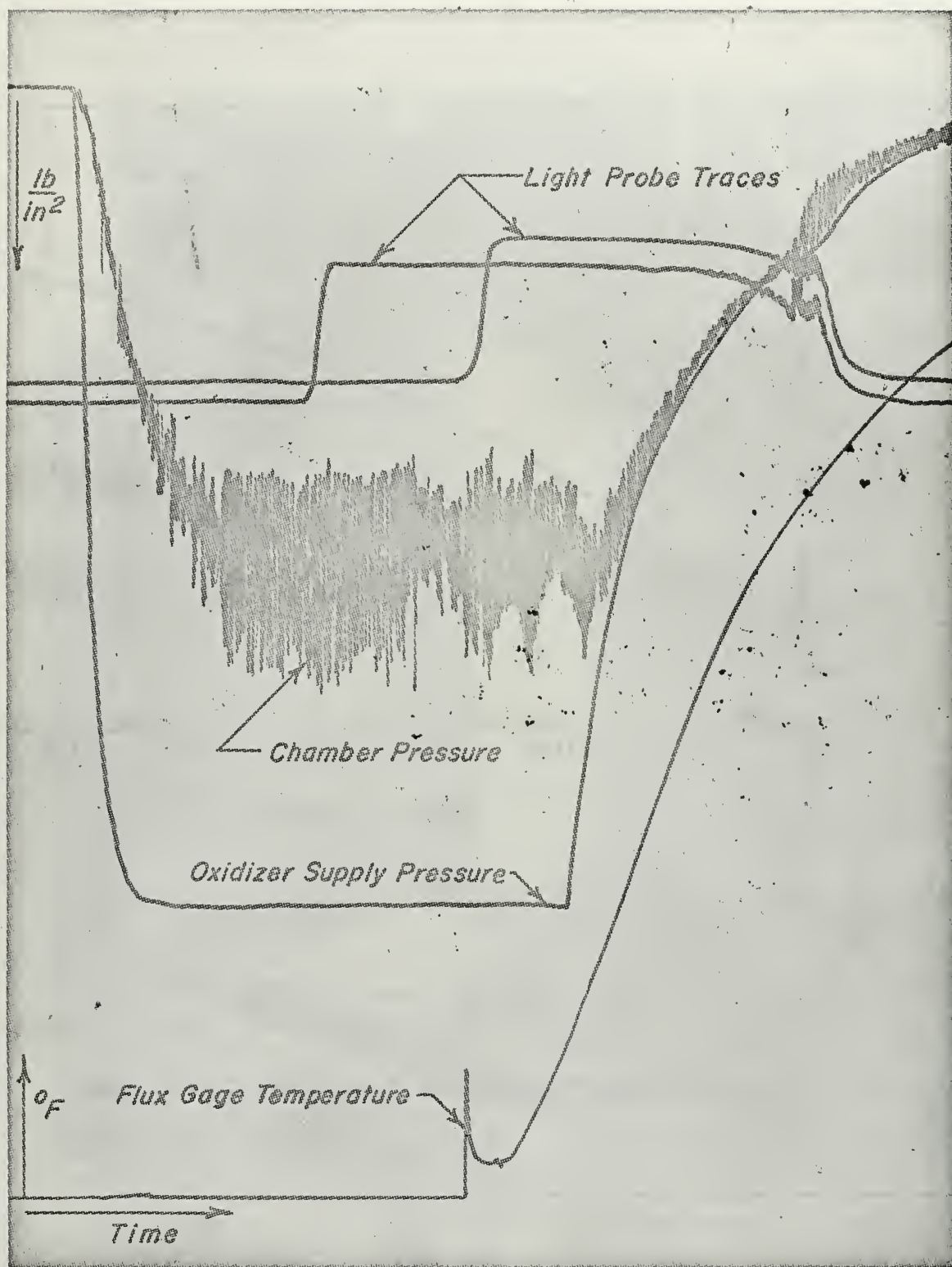


**Fig.17**  
**Typical Oscillograph Record**

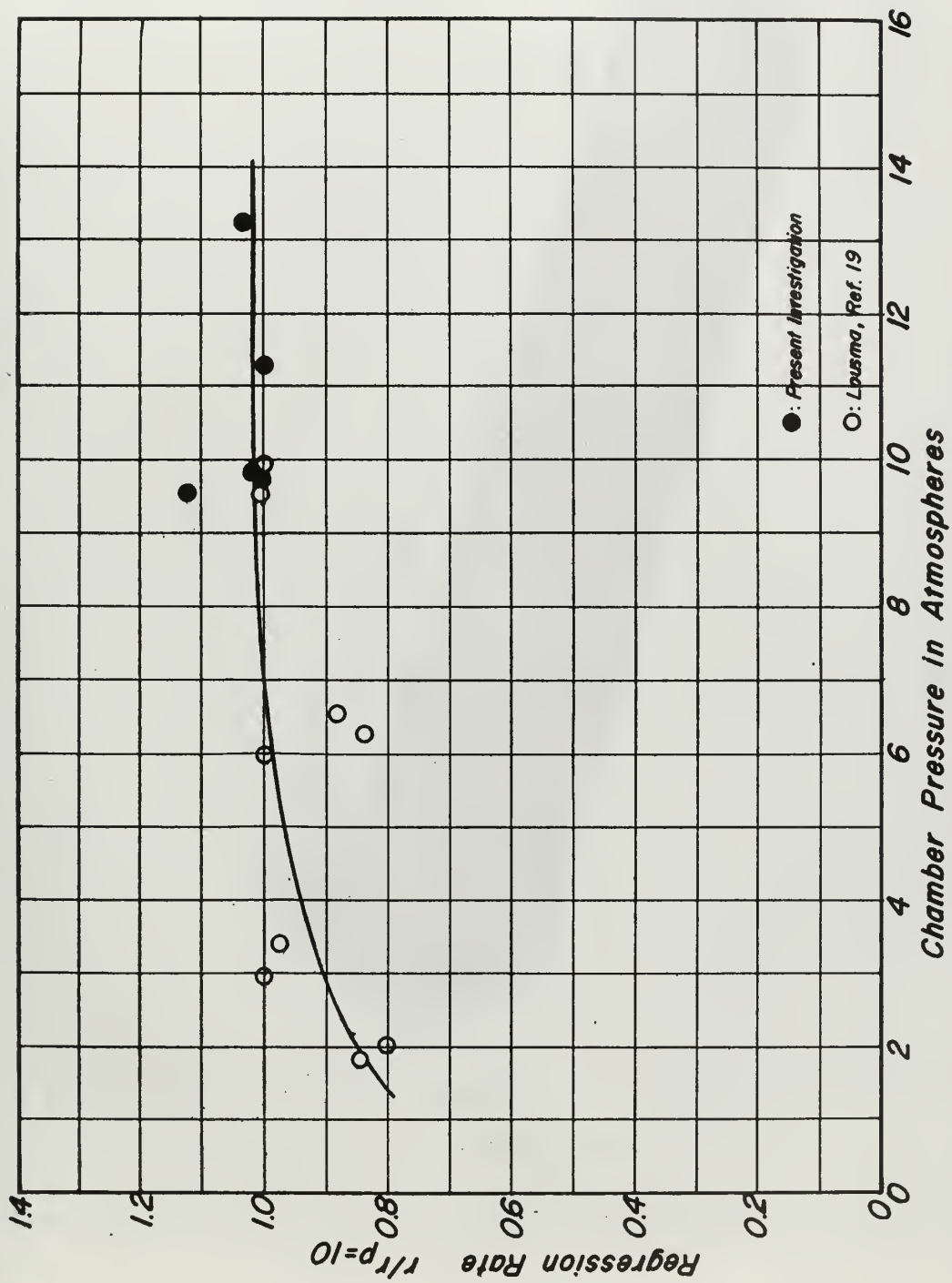
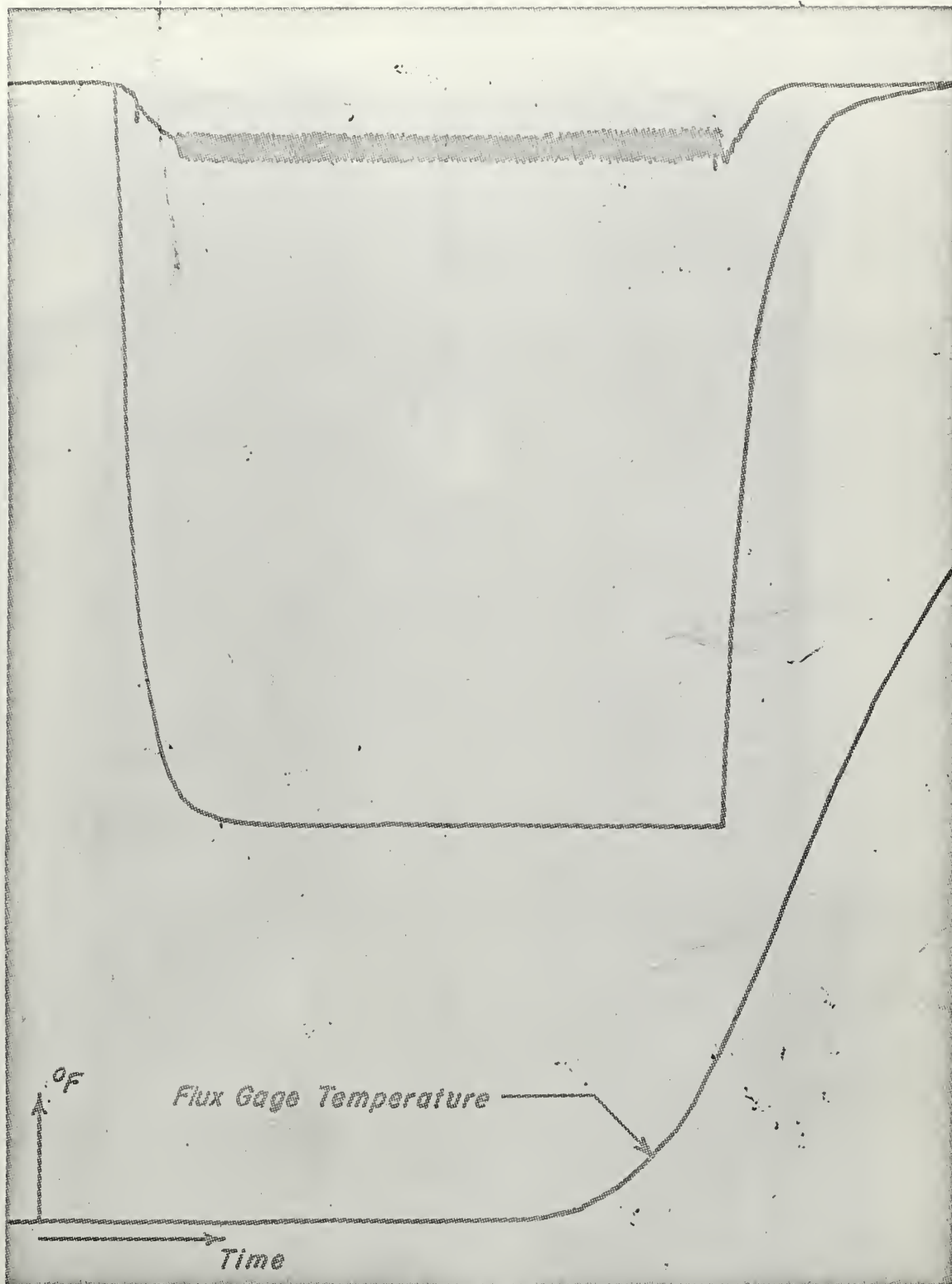


Fig.18 Normalized Regression Rates, Tubular Fuel Grain



*Fig. 19  
Mounted Slab Grain With Brass Fairing*



*Fig. 20*

*Oscillograph Record*

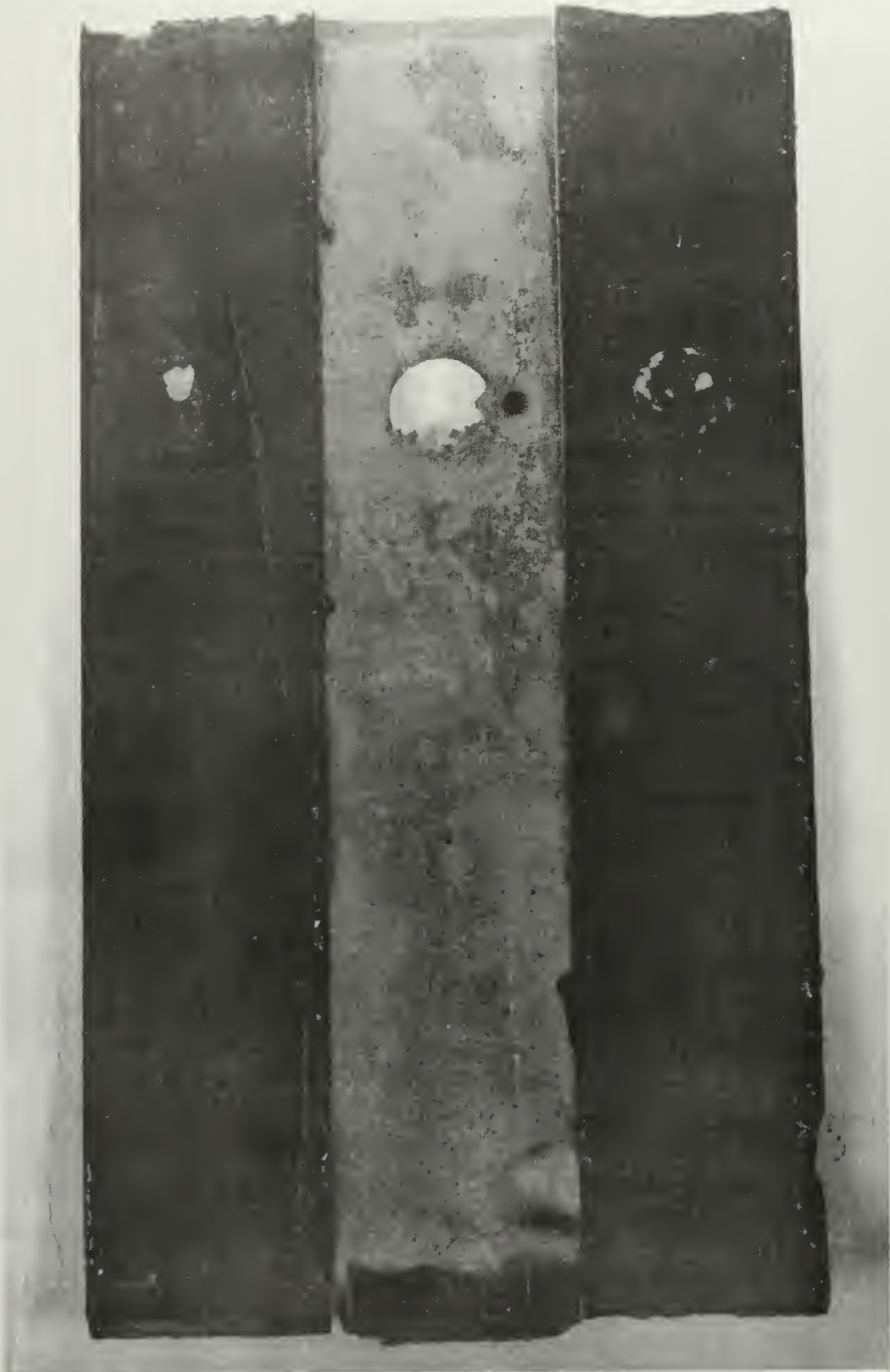


*Fig. 21 Incomplete Opening of Flux Gage Apertures*





*(a) Heavy Deposit From  
Aluminized Fuel*



*(b) Light Deposit From  
Aluminized Fuel*



*(c) Extreme Case of Soot Deposition From Polystyrene Fuel*

*Fig. 22 Combustion Product Deposits on Flux Gage Faces*

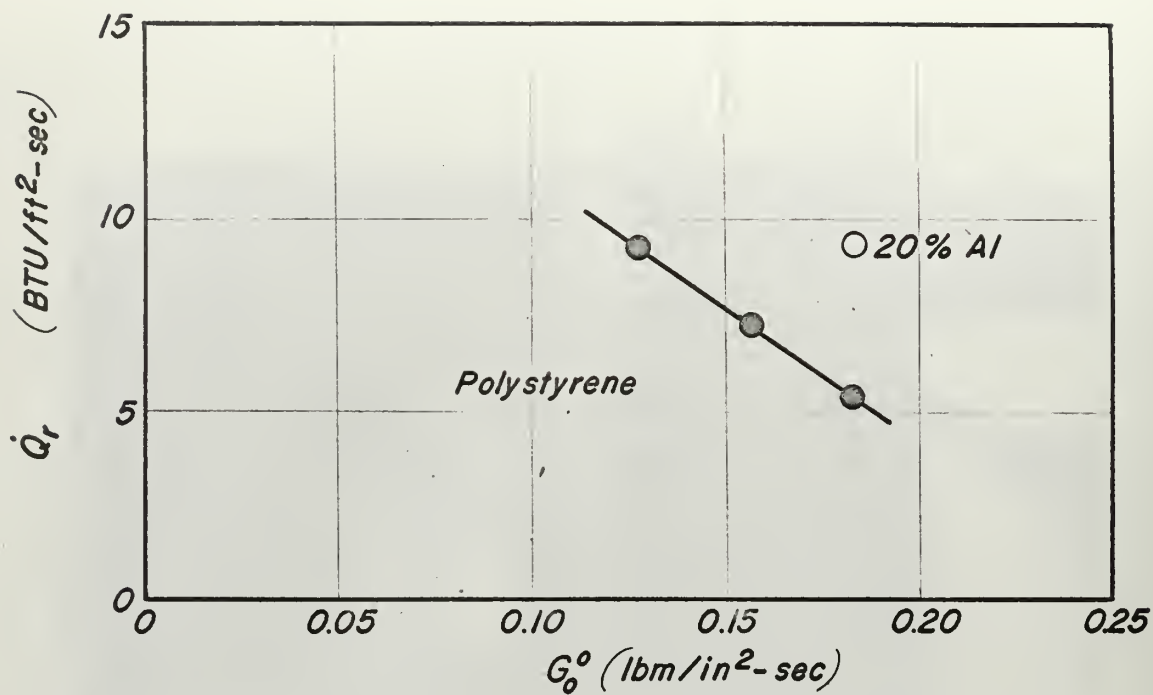


Fig. 23 Radiant Heat Flux vs Oxidizer Flow Rate

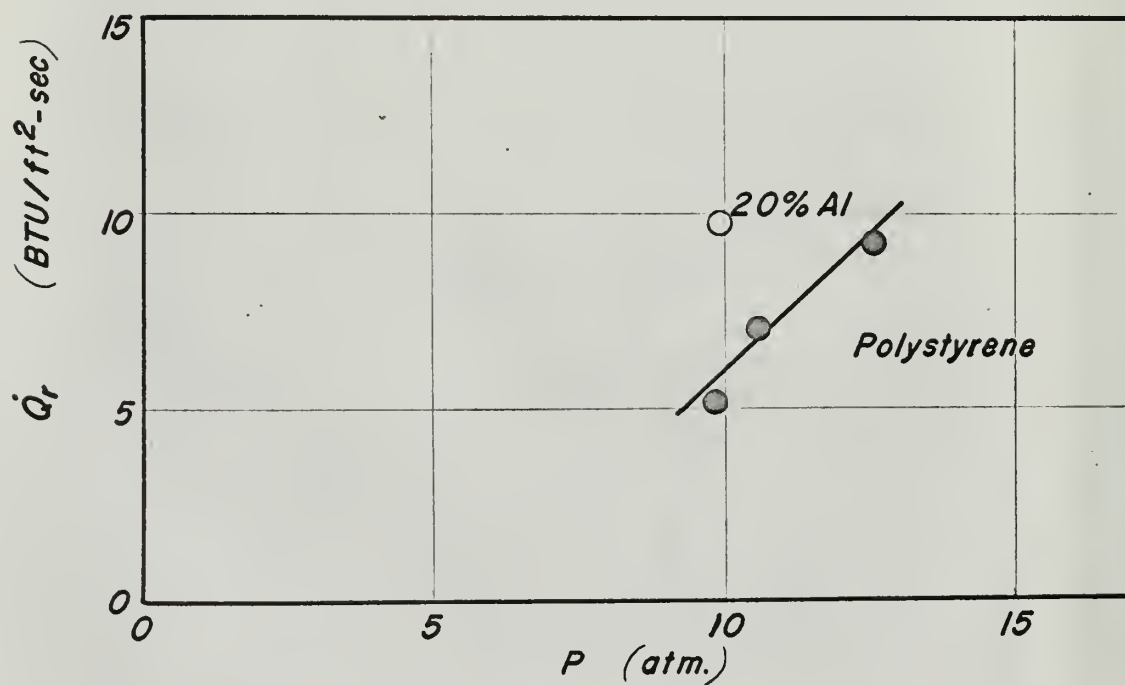
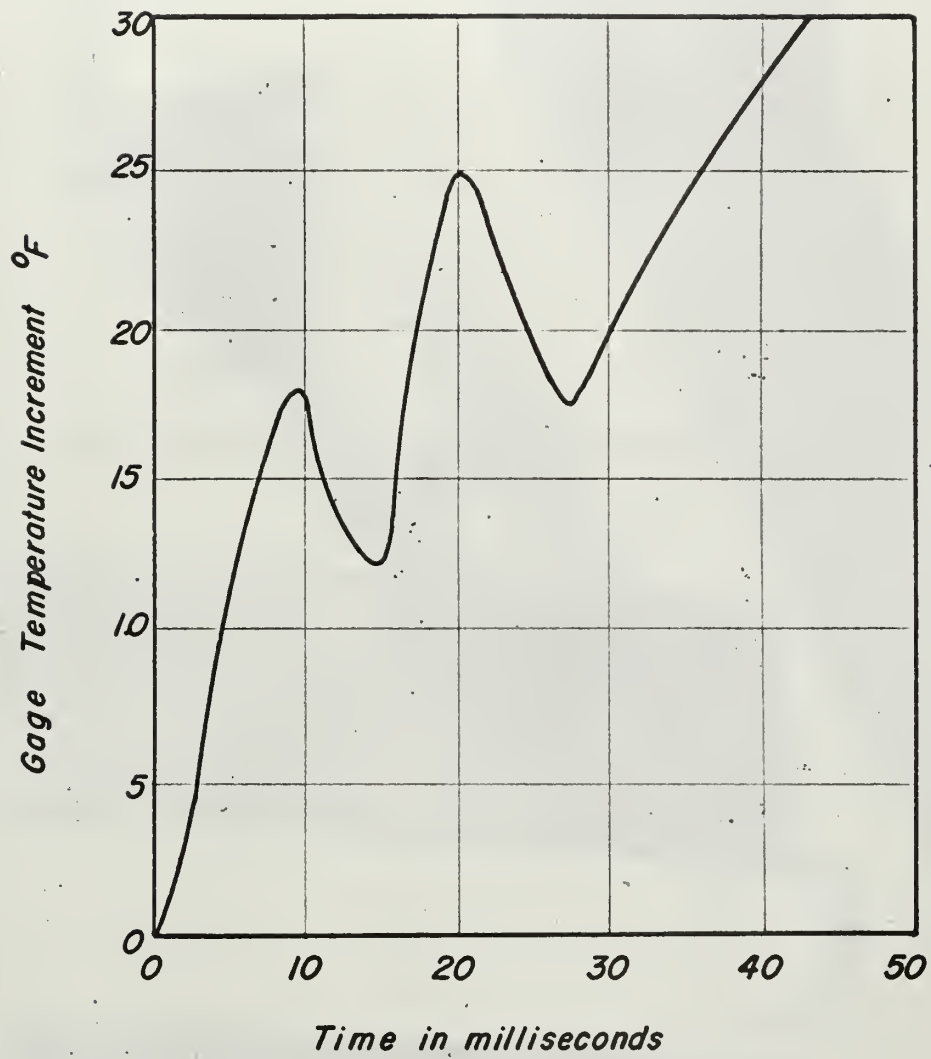


Fig. 24 Radiant Heat Flux vs Chamber Pressure



*Fig. 25*

*Example of Unsteady Heat Flux*



*(a) Damaged Steel Fairing, Top and Isometric Views*



*(b) Damaged and Undamaged Brass Leading Edge Fairing*

*Fig 26 Leading Edge Fairings*

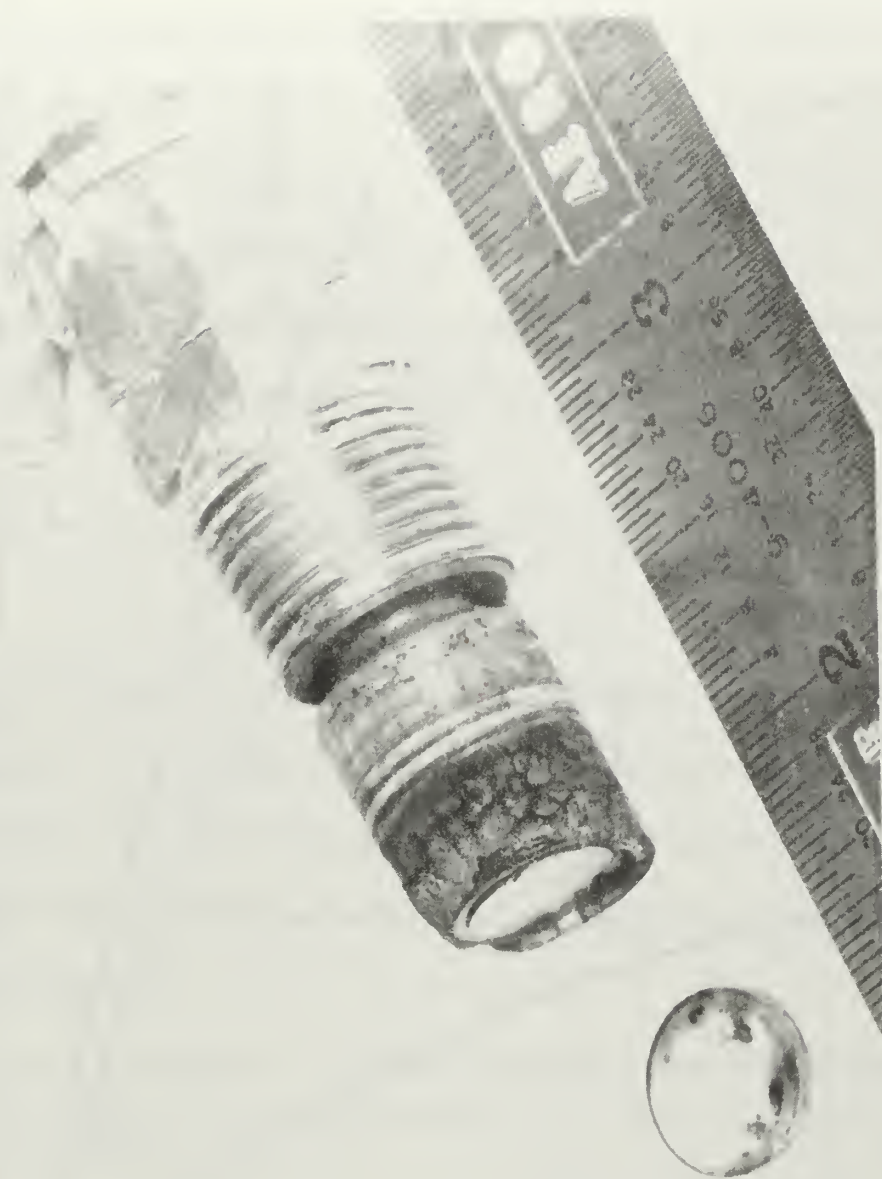


*Fig. 27 Destroyed Gage*



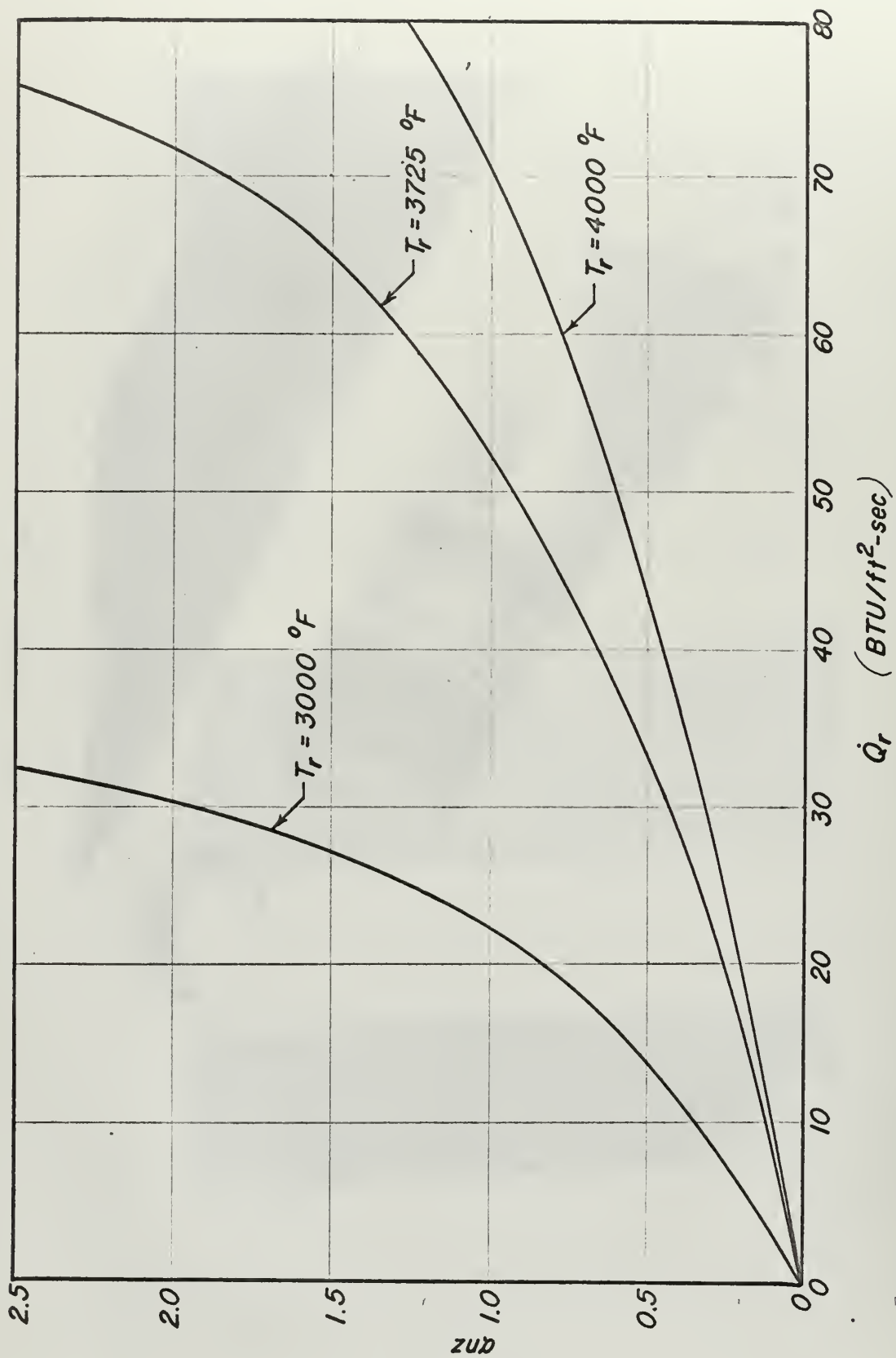


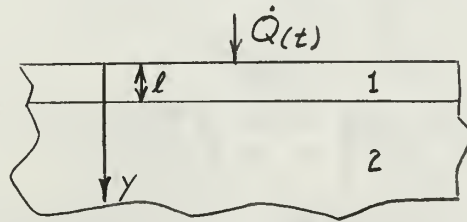
Fig.28 Heat Flux vs  $anz$

## APPENDIX I

### HEAT CONDUCTION THEORY

The thin film resistance thermometer measures the surface temperature of the substrate rather than heat transfer. However, the theory for heat conduction in a non-homogeneous solid can be used to relate the rate of heat transfer to the temperature history of the surface.

Following a development done by Vidal, a one dimensional model may be assumed as illustrated below.  $\overline{[1]}$  Here regions 1 and 2 represent



materials with different thermal properties. Region 1 is thin and the edge area of region 1 is much smaller than its plan-form area. Region 2 is assumed to be infinitely thick, an assumption which is valid for even relatively thin (1/16-inch) slabs of insulating material since region 1 is about four micro-inches in thickness.

Assuming heat transfer to be time dependent, the heat conduction equations for regions 1 and 2 are

$$\frac{\partial T_1}{\partial t} = \alpha_1 \frac{\partial^2 T_1}{\partial y^2}, \quad 0 \leq y \leq l, \quad (I-1)$$

where the applicable boundary conditions are

$$t \leq 0; \quad T_1(y) = 0$$

$$t > 0; \quad \left[ \frac{\partial T_1}{\partial y} \right]_{y=0} = - \frac{\dot{Q}(t)}{k_1},$$

and

$$\frac{\partial T_2}{\partial t} = \alpha_2 \frac{\partial^2 T_2}{\partial y^2} \quad l \leq y \leq \infty \quad (\text{I-2})$$

where

$$t \leq 0; \quad T_2(y) = 0$$

$$t > 0; \quad T_1(l) = T_2(l)$$

$$k_1 \left[ \frac{\partial T_1}{\partial y} \right]_{y=l} = k_2 \left[ \frac{\partial T_2}{\partial y} \right]_{y=l}$$

$$\lim_{y \rightarrow \infty} T_2 = 0$$

Here  $T_{(t)}$  is the increment of temperature above  $T_{(t \leq 0)}$ ,  $\alpha = \frac{k}{\rho c}$  is thermal diffusivity and  $\dot{Q}(t)$  is an arbitrary heat transfer rate to the surface.

The Laplace transforms of Eq. (I-1) and (I-2) and their boundary conditions are:

$$su = \alpha_1 \frac{d^2 u}{dy^2} \quad 0 \leq y \leq l \quad (\text{I-3})$$

with boundary conditions

$$y=0; \quad \left[ \frac{du}{dy} \right]_{y=0} = - \frac{\dot{Q}(s)}{k_1},$$

and

(I-4)

$$sv = \alpha_2 \left[ \frac{d^2 v}{dy^2} \right] ,$$

with boundary conditions:

$$y = l; \quad u = v$$

$$\left[ \frac{du}{dy} \right]_{y=l} = \frac{k_1}{k_2} \left[ \frac{dv}{dy} \right]_{y=l} ,$$

where  $u = \mathcal{L}\{T_1\}$ ,  $v = \mathcal{L}\{T_2\}$  and  $q_{\frac{1}{2}}(s) = \mathcal{L}\{\dot{Q}(t)\}$ .

The solutions to Eq. (I-3) and I-4) are given by

$$u = C_1 e^{y\sqrt{\frac{s}{\alpha_1}}} + C_2 e^{-y\sqrt{\frac{s}{\alpha_1}}} \quad (\text{I-5})$$

and

$$v = C_3 e^{y\sqrt{\frac{s}{\alpha_2}}} + C_4 e^{-y\sqrt{\frac{s}{\alpha_2}}} . \quad (\text{I-6})$$

Applying the boundary conditions to evaluate the arbitrary constants yields the transformed temperatures

$$u(s) = \frac{\alpha_1 q_{\frac{1}{2}}(s)}{k_1 \sqrt{s}} e^{-y\sqrt{\frac{s}{\alpha_1}}} \left[ \frac{1 + \sigma e^{-2(l-y)\sqrt{\frac{s}{\alpha_1}}}}{1 - \sigma e^{-2l\sqrt{\frac{s}{\alpha_1}}}} \right] \quad (\text{I-7})$$

and

$$V(s) = 1 + \frac{\sqrt{\alpha_1} q(s)}{k_1 \sqrt{s}} \sigma e^{-l\sqrt{\frac{s}{\alpha_1}}} \left[ \frac{e^{-(\gamma-l)\sqrt{\frac{s}{\alpha_1}}}}{1 - \sigma e^{-2l\sqrt{\frac{s}{\alpha_1}}}} \right], \quad (I-8)$$

where

$$\sigma = \frac{\sqrt{\frac{k_1 \rho_1 c_1}{k_2 \rho_2 c_2}} - 1}{\sqrt{\frac{k_1 \rho_1 c_1}{k_2 \rho_2 c_2}} + 1}$$

Inversion of Eq. (I-7) and (I-8) is accomplished by expanding the denominators in series for  $\sigma < 1$ . This expansion yields

$$U(s) = \frac{\sqrt{\alpha_1}}{k_1} \frac{q(s)}{\sqrt{s}} \left[ e^{-\gamma\sqrt{\frac{s}{\alpha_1}}} + \sum_{n=1}^{\infty} \sigma^n \left[ e^{-(2nl+\gamma)\sqrt{\frac{s}{\alpha_1}}} + e^{-(2nl-\gamma)\sqrt{\frac{s}{\alpha_1}}} \right] \right] \quad (I-9)$$

and



$$v_{(s)} = (1 + \sigma) \frac{\sqrt{\alpha_1} Q_{(s)}}{k_1 \sqrt{s}} e^{-(y-l)\sqrt{\frac{s}{\alpha_2}}} \cdot \sum_{n=0}^{\infty} \sigma^n e^{-(2n+1)l\sqrt{\frac{s}{\alpha_1}}} \quad (I-10)$$

These expressions are inverted to yield the temperatures

$$T_1(t) = \frac{1}{k_1} \sqrt{\frac{\alpha_1}{\pi}} \int_0^t \frac{\dot{Q}(\lambda)}{\sqrt{t-\lambda}} \exp\left[-\frac{y^2}{4\alpha_1(t-\lambda)}\right] d\lambda + \frac{1}{k_1} \sqrt{\frac{\alpha_1}{\pi}} \cdot \sum_{n=1}^{\infty} \sigma^n \int_0^t \frac{\dot{Q}(\lambda)}{\sqrt{t-\lambda}} \left[ \exp\left(-\frac{(2n\ell+y)^2}{4\alpha_1(t-\lambda)}\right) + \exp\left(-\frac{(2n\ell-y)^2}{4\alpha_1(t-\lambda)}\right) \right] d\lambda \quad (I-11)$$

$$T_2(t) = \left(\frac{1+\sigma}{k_1}\right) \sqrt{\frac{\alpha_1}{\pi}} \sum_{n=0}^{\infty} \sigma^n \int_0^t \left[ \frac{\dot{Q}(\lambda)}{\sqrt{t-\lambda}} \cdot \exp\left[-\frac{\left[(2n+1)\frac{\ell}{\sqrt{\alpha_1}} + \frac{y-\ell}{\sqrt{\alpha_2}}\right]^2}{4(t-\lambda)}\right] \right] d\lambda \quad (I-12)$$

Eq. (I-11) and (I-12) are exact solutions for the temperature distribution in a semi infinite body composed of two thermally dissimilar thermal properties such that  $\rho_1 c_1 k_1 < \rho_2 c_2 k_2$ . Obviously, calculation of  $\dot{Q}(t)$  from these equations would be rather complicated, hence some simplification is in order. The model described is characterized by  $\ell \ll 1$ ,  $k_1 \gg k_2$ , and the time intervals of interest are large compared with the characteristic time  $\ell^2/\alpha_1$ . With these characteristics it is valid to assume that the surface temperature and the measured  $T_{(t)}$  are the same and Eq. (I-11) becomes

$$\begin{aligned}
\left[ T(t) \right]_{y=0} &= \frac{1}{k_1} \sqrt{\frac{\alpha_1}{\pi}} \int_0^t \frac{\dot{Q}(\lambda)}{\sqrt{t-\lambda}} d\lambda \\
&+ \frac{1}{k_1} \sqrt{\frac{\alpha_1}{\pi}} \sum_{n=1}^{\infty} 2\sigma^n \cdot \int_0^t \left[ \frac{\dot{Q}(\lambda)}{\sqrt{t-\lambda}} \right. \\
&\cdot \exp \left[ - \frac{n^2 l^2}{\alpha_1 (t-\lambda)} \right] \Big] d\lambda .
\end{aligned} \tag{I-13}$$

The surface temperature is, from the above assumptions, seen to be essentially that of a homogeneous slab of material 2 with some correction necessary because of the presence of material 1. If the term

$$\frac{1}{k_1} \sqrt{\frac{\alpha_1}{\pi}} \sum_{n=1}^{\infty} 2\sigma^n \int_0^t \frac{\dot{Q}(\lambda)}{\sqrt{t-\lambda}} d\lambda$$

is added to and subtracted from Eq. (I-13), and note is made of the fact that

$$1 + \sum_{n=1}^{\infty} 2\sigma^n = \frac{1+\sigma}{1-\sigma} ,$$

Eq. (I-13) becomes

$$\begin{aligned}
\left[ T(t) \right]_{y=0} &= \frac{1}{\sqrt{\pi \rho_2 c_2 k_2}} \int_0^t \frac{\dot{Q}(\lambda)}{\sqrt{t-\lambda}} d\lambda - \frac{2}{\sqrt{\pi \rho_1 c_1 k_1}} \\
&\cdot \sum_{n=1}^{\infty} \sigma^n \int_0^t \frac{\dot{Q}(\lambda)}{\sqrt{t-\lambda}} \left[ 1 - e^{-\left[ \frac{n^2 \ell^2}{\alpha_1(t-\lambda)} \right]} \right] d\lambda . \quad (I-14)
\end{aligned}$$

The first term of Eq. (I-14) is seen to be the exact solution for the surface temperature of a homogeneous semi-infinite solid. The second term is a correction for the influence of the region 1. Integration of the correction term by parts and a subsequent series expansion yields

$$\begin{aligned}
&\frac{2}{\sqrt{\pi \rho_1 c_1 k_1}} \sum_{n=1}^{\infty} \sigma^n \int_0^t \frac{\dot{Q}(\lambda)}{\sqrt{t-\lambda}} \left[ 1 - e^{-\left[ \frac{n^2 \ell^2}{\alpha_1(t-\lambda)} \right]} \right] d\lambda \\
&= \frac{2}{\sqrt{\pi \rho_1 c_1 k_1}} \sum_{n=1}^{\infty} \sigma^n \left[ \int_0^t \frac{\dot{Q}(\lambda)}{\sqrt{t-\lambda}} \left[ 1 - e^{-\left[ \frac{n^2 \ell^2}{\alpha_1(t-\lambda)} \right]} \right] d\lambda \right. \\
&\quad \left. + n\ell \sqrt{\pi} \int_0^t \dot{Q}(\lambda) \left[ 1 - \operatorname{erf} \left( \frac{n\ell}{\sqrt{\alpha_1(t-\lambda)}} \right) \right] d\lambda \right] . \quad (I-15)
\end{aligned}$$

Expanding the exponential and error functions in Eq. (I-15) and substituting back into Eq. (I-14), and neglecting higher order terms in  $\ell$  yields an approximate solution for the surface temperature in the form

$$T(t) \cong \frac{1}{\sqrt{\pi \rho_2 c_2 k_2}} \int_0^t \frac{\dot{Q}(\lambda)}{\sqrt{t-\lambda}} d\lambda$$

$$- \dot{Q}(t) \left[ \frac{l}{k_1} \left( \frac{\rho_1 c_1 k_1}{\rho_2 c_2 k_2} - 1 \right) \right] . \quad (\text{I-16})$$

Inversion of Eq. (I-16) can be accomplished in closed form. However, it is expedient to adopt a more simple approach and obtain a solution involving iteration. This inversion has been accomplished by Vidal using Abel's integral equation for the inversion, integration by parts and subsequent differentiation to yield a form tractable for numerical calculations.  $\overline{[1]}$

This process, and the simplification to eliminate the slope of the temperature history curve from the calculation is tedious and will not be repeated here.

The resulting equation is

$$\dot{Q}(t) = \frac{\sqrt{\pi \rho_2 c_2 k_2}}{2} \left\{ \frac{T(t)}{\sqrt{t}} + \frac{1}{\pi \sqrt{t}} \right.$$

$$\cdot \int_0^t \frac{\sqrt{\lambda} T(t) - \sqrt{t} T(\lambda)}{(t-\lambda)^{3/2}} d\lambda + \frac{l}{\pi k_1} \left[ \frac{\rho_1 c_1 k_1}{\rho_2 c_2 k_2} - 1 \right] \quad (\text{I-17})$$

$$\cdot \left[ \frac{\dot{Q}(t)}{\sqrt{t}} + \frac{1}{2} \int_0^t \frac{\dot{Q}(t) - \dot{Q}(\lambda)}{(t-\lambda)^{3/2}} d\lambda \right] \Bigg\} .$$

It has been demonstrated that for films of the order of 1/10 micron thick the entire correction term can be neglected.  $\sqrt{\frac{1}{t}}$  Thus, to a first approximation the heat transfer rate is given by

$$\dot{Q}(t) = \frac{\sqrt{\pi \rho_2 c_2 k_2}}{2} \left[ \frac{T(t)}{\sqrt{t}} + \frac{1}{\pi \sqrt{t}} \int_0^t \frac{\sqrt{\lambda} T(t) - \sqrt{t} T(\lambda)}{(t-\lambda)^{3/2}} d\lambda \right]. \quad (I-18)$$

Correction for the presence of a window is necessary in the application of thin film thermometers to radiation measurement. External transmission of a slab of optical material is given by

$$\frac{I}{I_0} = (1-r)^2 e^{-ax} \quad (I-19)$$

where  $r$  = surface reflectivity,  $a$  = absorption coefficient, and  $x$  = window thickness.

Surface reflectivity is a function of index of refraction which varies with wave length of incident radiation,

$$r = \left( \frac{1-n}{1+n} \right)^2, \quad (I-20)$$

where  $n$  = index of refraction.  $n = 1.444$  for fused silica for wave lengths of one to two microns (infrared). From Eq. (I-20) then  $r = 0.033$ .  $a$  for



fused silica is  $\approx 0.01$  and for thickness  $x = 0.0625$  Eq. (I-19) yields

$$\frac{I}{I_0} = 0.935$$

with the assumption that  $e^{0.000625} \approx 1.0$ .

That is 93.5% of the incident radiation in the infrared and near infrared band will be transmitted by a fused silica window 1/16 inch thick.

# INITIAL DISTRIBUTION LIST

	No. Copies
1. Defense Documentation Center Cameron Station Alexandria, Virginia 22314	20
2. Library U. S. Naval Postgraduate School Monterey, California 93940	2
3. Commandant of the Marine Corps (Code A03C) Headquarters, U. S. Marine Corps Washington, D. C. 22214	1
4. Chairman, Department of Aeronautics U. S. Naval Postgraduate School Monterey, California 93940	2
5. Dr. R. E. Reichenbach, Department of Aeronautics U. S. Naval Postgraduate School Monterey, California 93940	5
6. Captain Henry L. Searle, USMC Rt. 2, Box 574 Yakima, Washington 98902	1
7. Mr. Leonard Bogdan Head, Instrumentation and Diagnostic Technique Section Applied Hypersonic Research Department Cornell Aeronautical Laboratory, Inc. Buffalo, New York 14221	1



## DOCUMENT CONTROL DATA - R&amp;D

(Security classification of title, body of abstract and indexing annotation must be entered when the overall report is classified)

1. ORIGINATING ACTIVITY (Corporate author) U. S. Naval Postgraduate School Monterey, California 93940		2a. REPORT SECURITY CLASSIFICATION Unclassified	
		2b. GROUP	
3. REPORT TITLE MEASUREMENT OF RADIANT HEAT TRANSFER TO THE FUEL GRAIN SURFACE IN A HYBRID ROCKET USING THIN FILM RESISTANCE THERMOMETERS			
4. DESCRIPTIVE NOTES (Type of report and inclusive dates)			
5. AUTHOR(S) (Last name, first name, initial) SEARLE, Henry L., Captain, USMC			
6. REPORT DATE May 1966	7a. TOTAL NO. OF PAGES 92	7b. NO. OF REFS 21	
8a. CONTRACT OR GRANT NO.	9a. ORIGINATOR'S REPORT NUMBER(S)		
b. PROJECT NO.			
c.	9b. OTHER REPORT NO(S) (Any other numbers that may be assigned this report)		
d.			
10. AVAILABILITY/LIMITATION NOTICES		This document has been approved for public release and sale; its distribution is unlimited.  Memorandum 11/25/69	
11. SUPPLEMENTARY NOTES None		12. SPONSORING MILITARY ACTIVITY Commandant of the Marine Corps (Code A03C) Headquarters, U. S. Marine Corps Washington, D. C. 22214	
13. ABSTRACT Measurement of the heat transfer to the pyrolyzing solid fuel surface is a necessary step in the continuation of analysis of hybrid rocket combustion phenomena. Thin film resistance thermometers were used to measure the radiative component of energy transfer from the flame zone to the fuel surface. A slab grain combustion chamber, which provided a planar flame zone in a flat plate boundary layer, was designed and utilized in this investigation. The existing hybrid rocket test apparatus was also used after extensive redesign of the supply, control, and instrumentation systems. Fuels studied were polystyrene and aluminum filled plexiglas with oxygen used as oxidizer. Radiant heat flux values were obtained in the slab burner at chamber pressures from nine to fifteen atmospheres with oxidizer flow rates above 0.15 lbm/in <sup>2</sup> -sec. Radiant energy transfer to the fuel surface appears to increase with pressure and decrease with oxidizer flux as expected.			



14. KEY WORDS	LINK A		LINK B		LINK C	
	ROLE	WT	ROLE	WT	ROLE	WT
Measurement, Heat Transfer, Hybrid, Propulsion, Combustion, Gage, Radiation						

## INSTRUCTIONS

1. **ORIGINATING ACTIVITY:** Enter the name and address of the contractor, subcontractor, grantee, Department of Defense activity or other organization (*corporate author*) issuing the report.

2a. **REPORT SECURITY CLASSIFICATION:** Enter the overall security classification of the report. Indicate whether "Restricted Data" is included. Marking is to be in accordance with appropriate security regulations.

2b. **GROUP:** Automatic downgrading is specified in DoD Directive 5200.10 and Armed Forces Industrial Manual. Enter the group number. Also, when applicable, show that optional markings have been used for Group 3 and Group 4 as authorized.

3. **REPORT TITLE:** Enter the complete report title in all capital letters. Titles in all cases should be unclassified. If a meaningful title cannot be selected without classification, show title classification in all capitals in parenthesis immediately following the title.

4. **DESCRIPTIVE NOTES:** If appropriate, enter the type of report, e.g., interim, progress, summary, annual, or final. Give the inclusive dates when a specific reporting period is covered.

5. **AUTHOR(S):** Enter the name(s) of author(s) as shown on or in the report. Enter last name, first name, middle initial. If military, show rank and branch of service. The name of the principal author is an absolute minimum requirement.

6. **REPORT DATE:** Enter the date of the report as day, month, year; or month, year. If more than one date appears on the report, use date of publication.

7a. **TOTAL NUMBER OF PAGES:** The total page count should follow normal pagination procedures, i.e., enter the number of pages containing information.

7b. **NUMBER OF REFERENCES:** Enter the total number of references cited in the report.

8a. **CONTRACT OR GRANT NUMBER:** If appropriate, enter the applicable number of the contract or grant under which the report was written.

8b, 8c, & 8d. **PROJECT NUMBER:** Enter the appropriate military department identification, such as project number, subproject number, system numbers, task number, etc.

9a. **ORIGINATOR'S REPORT NUMBER(S):** Enter the official report number by which the document will be identified and controlled by the originating activity. This number must be unique to this report.

9b. **OTHER REPORT NUMBER(S):** If the report has been assigned any other report numbers (*either by the originator or by the sponsor*), also enter this number(s).

10. **AVAILABILITY/LIMITATION NOTICES:** Enter any limitations on further dissemination of the report, other than those

imposed by security classification, using standard statements such as:

- (1) "Qualified requesters may obtain copies of this report from DDC."
- (2) "Foreign announcement and dissemination of this report by DDC is not authorized."
- (3) "U. S. Government agencies may obtain copies of this report directly from DDC. Other qualified DDC users shall request through \_\_\_\_\_."
- (4) "U. S. military agencies may obtain copies of this report directly from DDC. Other qualified users shall request through \_\_\_\_\_."
- (5) "All distribution of this report is controlled. Qualified DDC users shall request through \_\_\_\_\_."

If the report has been furnished to the Office of Technical Services, Department of Commerce, for sale to the public, indicate this fact and enter the price, if known.

11. **SUPPLEMENTARY NOTES:** Use for additional explanatory notes.

12. **SPONSORING MILITARY ACTIVITY:** Enter the name of the departmental project office or laboratory sponsoring (*paying for*) the research and development. Include address.

13. **ABSTRACT:** Enter an abstract giving a brief and factual summary of the document indicative of the report, even though it may also appear elsewhere in the body of the technical report. If additional space is required, a continuation sheet shall be attached.

It is highly desirable that the abstract of classified reports be unclassified. Each paragraph of the abstract shall end with an indication of the military security classification of the information in the paragraph, represented as (TS), (S), (C), or (U).

There is no limitation on the length of the abstract. However, the suggested length is from 150 to 225 words.

14. **KEY WORDS:** Key words are technically meaningful terms or short phrases that characterize a report and may be used as index entries for cataloging the report. Key words must be selected so that no security classification is required. Identifiers, such as equipment model designation, trade name, military project code name, geographic location, may be used as key words but will be followed by an indication of technical context. The assignment of links, roles, and weights is optional.









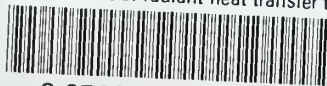






thesS4057

Measurement of radiant heat transfer to



3 2768 001 94435 8

DUDLEY KNOX LIBRARY